Growing Ice in a Tank: Young Sea Ice Evolution and Turbulence in the Under Ice Boundary Layer

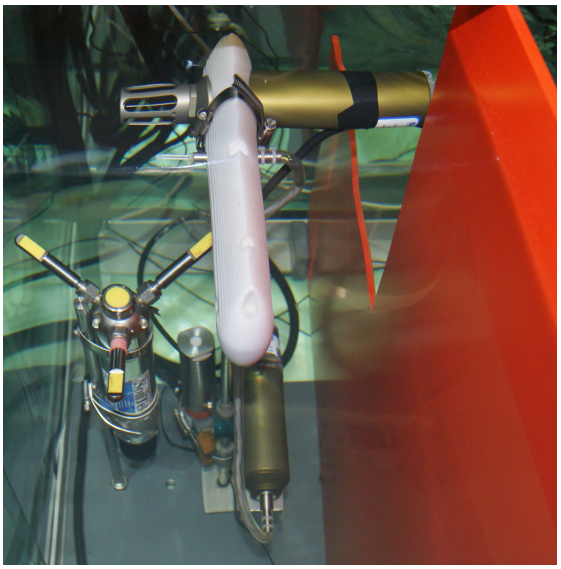

Master's Thesis in Physical Oceanography

Lisbeth Håvik

November 2011

Abstract

Thin sea ice and its modifications of the oceanic boundary layer are important in the context of the recent retreat of the Arctic sea ice cover. To study turbulence in the under ice boundary layer during thin sea ice growth, tank experiments in an ice laboratory were conducted under varying atmospheric and oceanographic conditions. Two main groups of experiments were investigated; circular current and stagnant water. Salinity data revealed that the ice releases brine both during freezing and melting conditions, before the solid ice starts melting. Four different methods were tested to quantify heat and salt fluxes. The covariance method underestimated the fluxes with up to two orders of magnitude, and hence did not resolve the fluxes present in the tank. The turbulent kinetic energy budget suggests non-uniform turbulence in the tank, leading to large differences in sources and sinks of turbulence over the relatively small surface area. The typical mixing length decreased downstream from 0.06 m to 0.03 m over a horizontal distance of 43 cm. Brine plumes leaving the ice were detected during all experiments, and enhanced the upper ocean mixing. The total importance of the large instantaneous salt and heat fluxes during brine plumes was less than 3 %, and did not considerably affect the heat and salt budgets in the tank.

Acknowledgements

I would very much like to thank my supervisor, Anders Sirevaag, for all help with this thesis and for giving me an eventful year! He gave me the possibility to do laboratory work in Hamburg, introduced me for the Norwegian Polar Institute leading to a cruise in the Arctic, and encouraged me to attend the ResClim Summer School in Svalbard. He has been an available supervisor, open for questions and discussions and it was always pleasant to visit his office. I would also like to thank my co-supervisor Dirk Notz for valuable feedback and lots of ideas during this work, and for taking good care of me the time I spent in Hamburg. The weeks I spent in Hamburg would not have been the same without Ann Kristin Naumann. Thanks for a very good cooperation in the laboratory and for bringing me to concerts, drinks and dinners. A special thanks to those of my friends that have taken their time to read through my thesis and giving me feedback.

To my great family and friends: I have had the time of my life these last five years, thank you!

Contents

1

Introduction

Sea ice covers almost 12 % of the world oceans [Weeks, 2010]. It is relatively thin and has a small volume, but due to its modifications of the interaction between atmosphere and ocean, it plays a significant role in the global climate and has become one of the most important components in climate research [Dieckmann and Hellmer, 2003]. Due to its high albedo sea ice reflects incoming solar radiation more efficiently than open water, and makes a large difference in the ocean-ice-albedo feedback during summer [Comiso, 2002]. Over the last years the sea ice cover in the Arctic Ocean has been retreating rapidly [Stroeve et al., 2007]. Larger and larger areas have become ice free every summer, and this is suggested to continue in a warming climate [Comiso et al., 2008]. A possible ice free Arctic in the summer months increases the interest of understanding the processes governing the thin ice growth in the following autumn, and has been a motivation for this work.

Open water and thin ice affect the thermohaline structure of the upper ocean more than the perennial ice pack by a rapid cooling of the water by the atmosphere, and release of salt to the underlying ocean during ice freezing. Both the strong cooling from above and brine release from ice formation will make the surface layer denser than underlying water masses. An unstable stratification with dense, cold and saline water on top of lighter, warmer and fresher water leads to convection and mixing in the ocean boundary layer [Eicken, 2003]. These water mass transformations through melting and freezing of sea ice at high latitudes change the thermohaline structure of the ocean, and are important for the thermohaline circulation in the world oceans

[Aagaard and Carmack, 1989].

The mechanism for forming sea ice from open water is different from thickening of already existing ice, and hence affects the upper ocean boundary layer in a different way. In initially open water, frazil ice crystals form in the top decimetres of the water column [Wadhams, 2000], and are at first kept in suspension by wind and wave generated turbulence in the upper ocean. As their concentration increase they accumulate at the surface and the mix of crystals and water freezes up to a solid-ice cover. In presence of turbulence from the wave field, consolidated pieces of ice called pancake ice form.

Thin sea ice is important for the surface mass and heat balance in the Arctic Ocean [Wettlaufer et al., 2000], and is present in the marginal ice zone and in leads in the perennial ice cover. Maykut [1982] found that young sea ice has to be included in the salt budget to obtain the salinity development observed in the mixed layer. Even if leads only cover a small area of the Arctic Ocean, the salt release from refreezing of leads is suggested by Morison and Smith [1981] to redistribute over a large area. Since brine leaves the ice abruptly after growing for some time [Wettlaufer et al., 2000], the growth process is a source of turbulence in the oceanic boundary layer. The most common and practical way to investigate refreezing of leads, thin ice growth and the following convection, are through numerical simulations and laboratory experiments [Wettlaufer et al., 2000]. De La Rosa et al. [2011] analysed the frazil pancake cycle of ice grown from saline water in a tank. They studied temperature of air, ice and water together with salinity of ice and water to understand the thermodynamics and morphological cycle of ice growth. They show decreasing salinity for the frazil crystals and pancake ice with time, and indicate a very strong decay in salinity in the first few hours of growth.

These earlier studies raise the interest of being able to study the boundary layer underneath sea ice during the initial salt release from the ice. For newly formed ice in the ocean it is hard to measure the turbulent fluxes directly, since one does not have a solid platform to fix instrumentation to. In field campaigns in the Arctic, turbulence instrumentation have been used for thicker ice where it can be mounted from the ice during the measurement period [McPhee and Stanton, 1996]. A laboratory setup defines a unique opportunity to measure the fluxes under thin ice, and the transition from open water to a solid ice cover and back again.

During two measurement periods, two weeks in November 2010 and four weeks in February 2011, experiments were performed in an ice laboratory at Max Planck Institute for Meteorology, Hamburg. The first period of two weeks was used to test the

instrumentation and the tank layout by conducting six test experiments to learn how the setup would work best. The last period was the main experiment period, where several experiments were performed to gain deeper insight into the processes in the under-ice boundary layer. The experiments were conducted to study growth of thin ice from saline water under varying atmospheric and oceanic conditions. The aim was to better understand and quantify the upper ocean mixing underneath growing sea ice in the initial phase from cooling down the water to the freezing point and the first hours of freezing, as well as melting of thin ice and the transition back to open water. In addition, the instrumentation used had not been tested in a tank study before, and the validation of the measurements was important. Fluxes of salt, heat and momentum are known processes that modify the properties of the under ice boundary layer and by measuring 3-D velocity, temperature and conductivity at relatively high frequencies for varying environmental conditions, the transfer of heat and salt at the ice ocean interface could be quantified. The difference between ice formation in calm water and frazil ice crystal production in turbulent water was compared in terms of salt and heat fluxes by using different estimation techniques. Brine plumes leaving the ice enhance the upper ocean mixing, and their dynamics and impact on the total heat and salt budgets were examined.

In the next chapter a theoretical background of sea ice and ocean turbulence used in this thesis will be presented. Chapter 3 contains a description of the experiment setup and how the experiments were accomplished, together with a description of the instrumentation and the different methods used. The results are presented in Chapter 4 and discussed in Chapter 5. Chapter 6 summarises the work, and gives a short outlook.

2

Theory

This chapter introduces some background theory of sea ice in the first section, including how sea ice grows under different environmental conditions and the desalination processes leading to brine release. In the last section, theory of ocean turbulence is introduced to give a short overview of basic properties of turbulence, and how freezing and melting of sea ice affects the turbulent fluxes in water.

2.1 Sea ice

As sea water is cooled from above by the atmosphere the density increases. Surface water sinks down and is replaced by lighter water from below, inducing a thermohaline convection [Eicken, 2003]. For salinities exceeding 24.7 g/kg, cooling of water towards the freezing point will always lead to an increase in density of the surface layer [Wadhams, 2000], and theoretically convection will continue until the freezing point is reached for the entire water column. Freezing point of sea water is depressed relative to that of fresh water because of the dissolved salts. A salinity of 34 g/kg corresponds to a freezing point of -1.86 °C [Eicken, 2003], and a further increase in salinity will lead to a lowering of the freezing point. If the whole ocean was well mixed the convection would have to go all the way to the bottom, and the entire water column would be at the freezing point before sea ice formation could start. Because of the vast amount of heat in the ocean no sea ice cover would then have formed, and the ocean would have remained ice free. In the Arctic Ocean there is typically a cold layer with a strong

salinity gradient in the upper few tens of metres, called the cold halocline layer [Aagaard et al., 1981]. This separates the surface layer from the layer underneath [Steele and Boyd, 1998] and when convection reaches this depth the water is again less dense than the water below, and convection would not go any deeper. When all the water above the halocline is at the freezing point, a further cooling at the surface will lead to formation of sea ice.

Sea ice is a two-phase medium consisting of both fresh solid ice and highly saline and liquid brine. The dissolved salts in sea water can not be included in the solid ice crystal structure and are expelled into remaining water, which together makes up the liquid brine, situated in the brine channel system existing in the ice. The freezing point of brine is depressed relative to that of sea water, and dependent on the brine salinity, which is again entirely governed by temperature [Notz, 2005]. When ice becomes colder more of the liquid brine freezes, and an increasing amount of salt is included in the reduced volume of the remaining brine. Vice versa for warmer sea ice, the brine is more diluted and makes up a larger portion of the total volume.

Various parameters are used to describe sea ice and its physical properties. The solid mass fraction ϕ is a measure of how large part of the sea ice is frozen in pure ice. This can be expressed as the relationship between the mass of the solid ice m_s and the total mass m, $\phi = \frac{m_s}{m}$, where the total mass $m = m_s + m_{br}$ is the sum of the mass of the solid ice and the mass of the brine. The bulk salinity S_{bu} of sea ice is considerably lower than the salinity of the water from which it is grown. A typical S_{bu} of young sea ice is 10 g/kg [Wadhams, 2000], and as the ice grows older this value is reduced by mechanisms explained in Section 2.1.2. The bulk salinity of the ice can be expressed as

$$mS_{bu} = m_s S_s + m_{br} S_{br}, \tag{2.1.1}$$

where the salinity of the solid ice $S_s = 0$ g/kg. The brine salinity S_{br} is the salinity of the cold and dense liquid contained in the brine channel system of the ice and can be expressed for NaCl solutions by a polynomial [Notz, 2005] as

$$S_{br} = -17.6T - 0.389T^2 - 0.00362T^3. \tag{2.1.2}$$

The solid fraction is linked to the brine salinity S_{br} and bulk salinity S_{bu} through

$$\phi = 1 - \frac{S_{bu}}{S_{br}}, \tag{2.1.3}$$

following from $m = m_s + m_{br}$ and equation 2.1.1. At low temperatures sea ice will have a larger solid fraction than at warmer temperatures and the brine will also have a higher salinity.

2.1.1 Ice formation

When sea ice first forms in entirely calm conditions, large crystals float on the water surface. They are fragile and easily affected by any turbulence. If the water is calm, the crystals rapidly freeze together and form a transparent ice cover called nilas [Wadhams, 2000]. The ocean is seldom calm enough for growth of transparent nilas in the marginal ice zone or open ocean, and only small leads under calm conditions will grow in this way. In the presence of any turbulence, the crystals will be broken into frazil crystals and suspended in the top decimetres of the water [Eicken, 2003]. The frazil ice crystal density increases with a further cooling from the atmosphere, and eventually freeze together as a continuous thin ice cover. When this first continuous ice cover is formed a further increase in thickness is through congelation growth, where ice crystals freeze on already existing ice from underneath [Wadhams, 2000].

In rough water the frazil crystals grow for a longer period before a solid ice cover is formed. This gives a thick slush layer moving with the waves in a cyclic motion [Wadhams, 2000]. When the solid fraction of the slush layer reaches 30-40 % [Martin and Kaufmann, 1981], the crystals can freeze together and form small cakes of ice called pancake ice, of typical size of some decimetres to some metres [Notz, 2005]. Between the pancakes there are still frazil crystals in the water which can freeze on the pancakes and make them grow in size. Since the ice cover is not continuous the heat flux between the atmosphere and the underlying water is large [Smedsrud, 2011], and can efficiently remove the latent heat released by freezing. Eventually the pancakes will freeze together and make larger floes.

2.1.2 Brine release mechanisms

Formation of sea ice releases saline brine to the underlying ocean and is controlling the buoyancy forcing at the surface of polar oceans [Comiso, 2008]. This salt release enhances the upper ocean mixing [Wettlaufer et al., 2000], and is found by Notz and Worster [2009] to be governed by two mechanisms dependent on which season it is. In winter, when no surface melting occurs, the only significant loss of brine is through

gravity drainage. The temperature of the atmosphere is lower than that of the ocean, which leads to a temperature gradient in the ice. Cold ice on top of warmer ice leads to an unstable density gradient in the brine cells, with saltier and colder brine at the top and fresher and warmer brine at the bottom. As the ice grows thicker, the saline brine drains out through the brine channels due to gravity and leaves the ice through the base. Fresher sea water with a higher freezing point will replace the brine, and a freeze up of the brine channels will take place to maintain thermodynamic stability. This process will not occur immediately after freezing has started, and the onset can be described by the Rayleigh number [Wettlaufer et al., 1997], a dimensionless parameter associated with buoyancy driven flow. It is given as the ratio of available potential energy, due to density difference in the brine, to the dissipative forces in diffusion and viscosity. This can be expressed as

$$Ra = \frac{g(\rho_{br} - \rho_w)\Pi h}{\kappa\mu}, \tag{2.1.4}$$

where g is the gravitational constant, ρ_{br} is the density of the liquid brine, ρ_w is the density of the underlying sea water, h is the ice thickness, κ is the thermal diffusivity and μ is the dynamic viscosity of the brine [Notz, 2005]. Π is the permeability, dependent on the solid volume fraction ϕ_v, and can be calculated from the empirically determined formula for young sea ice found by Freitag [1999],

$$\Pi = 10^{-17}[10^3(1 - \phi_v)]^{3.1}. \tag{2.1.5}$$

Convection in the brine channels is decided by the difference in density between brine and seawater and if Ra exceeds a critical value, Ra_c, close to 10 [Notz and Worster, 2008], convection will start in the brine pockets and S_{bu} will decrease due to gravity drainage.

During summer sea ice can also become fresher through flushing of fresh melt water percolating the ice from melt ponds. The percolation drives the salt out of the ice through the brine channels. They are then filled with fresh melt water with a higher freezing point than the brine, and the channels freeze up and the ice gets less permeable. If an ice floe survives the summer melting it will be stronger the next summer, because of a lower liquid fraction.

2.2 Ocean Turbulence

Turbulence is the dominating physical process in transfer of heat, momentum and salt in the ocean [Thorpe, 2007]. It is energetic and disperses properties of fluid elements at far higher rates than the molecular diffusivity [Stull, 2008]. By stretching water elements the area where molecular diffusion can transfer properties such as salt and temperature is increased, and together dispersion and diffusion mixes water much more efficiently than diffusion alone [Thorpe, 2007]. The Reynolds number is a measure of turbulence and is defined as

$$Re = \frac{U \cdot l}{\nu}, \tag{2.2.1}$$

where U is the typical velocity scale, l is a typical length scale and ν is the kinematic viscosity. When the Reynolds number exceeds ~ 1000 the flow will be turbulent. Typical values of U, l and ν in the ocean gives large Re, and the ocean is always considered to be turbulent.

Turbulence can not be described deterministic because of its random and irregular nature. Instead statistical properties such as mean, variance and covariance are used to give a quantitative description. The energy spectrum of turbulence is broad, and different scales of eddies are involved. Most of the energy is contained in the large eddies, and dissipation of turbulent kinetic energy occurs at a small scale. Dissipation is transfer of kinetic energy to heat through viscous shear. Large-scale variations need to be isolated from the fluctuating parts in order to study turbulence. By using Reynold's averaging over longer time periods one can obtain the mean of the fluctuations and then subtract this from the instantaneous values to obtain the turbulent part. For temperature e.g.

$$T' = T - \overline{T}, \tag{2.2.2}$$

where T' represents the turbulent part, T the instantaneous value and $\overline{T}$ the time mean. This can be done similarly for other scalar properties and velocity components.

2.2.1 Turbulence spectrum and energy cascade

Spectral analysis is useful to study the energy cascade from larger eddies towards the smaller ones in a turbulent flow [McPhee, 2008a]. Turbulence spectra are usually broad and cover a large range of frequencies and intensities. Typically the lowest frequencies represent the large energy-containing eddies, intermediate frequencies are associated

with the inertial subrange and the highest frequencies represent dissipation of energy to heat [Stull, 2008]. A typical turbulence spectrum is displayed in a log-log plot to best cover the range of frequencies and spectral densities [Stull, 2008]. In the inertial subrange the eddies get their energy from the larger eddies and loose their energy in the same way to smaller eddies, hence there is no net energy supply in this frequency range. This indicates that the energy cascade down the spectrum must be balanced by dissipation (ϵ) at the smallest levels for a steady-state turbulent flow [Stull, 2008].

By using continuous spectral representations it is assumed that there is a spectral energy density, e.g. for vertical velocity $S_{ww}(f)$, that can be integrated over all frequencies to get the total variance [Stull, 2008]

$$\sigma_w^2 = \int_f S_{ww}(f)df. \tag{2.2.3}$$

The spectral energy density has units of velocity squared per unit frequency. The frequency (f) can be transformed to wavenumber (k) through $k = 2\pi f/U$, where U is the mean flow velocity. For discrete k this spectral kinetic energy density for a single velocity component $\phi_w(k)$ can be given as a function of ϵ, k and the Kolmogorov constant $q = 0.51$ [McPhee, 2008a],

$$\phi_w(k) = q\epsilon^{2/3}k^{-5/3}, \tag{2.2.4}$$

in the inertial subrange, where the inertial dominate over viscous forces [Thorpe, 2007]. A power law relationship in a turbulence spectrum appears as a strait line, which in the inertial subrange is proportional to $k^{-5/3}$. The turbulence spectra can be used to validate the turbulent measurements, and serve as a check if turbulence is well developed [McPhee, 2008a].

Figure 2.1 shows a typical energy spectrum for vertical velocity. It is presented as a weighted spectrum through a modification of equation 2.2.4,

$$k\phi_w(k) = q\epsilon^{2/3}k^{-2/3}, \tag{2.2.5}$$

with the units of variance. The $k^{-2/3}$ dependency is visible in the weighted spectrum as a constant gradient at wavenumbers in the inertial subrange. This can be used to calculate ϵ for a given k in this region by reading the corresponding values for k and $k\phi_w(k)$ from the graph, and using equation 2.2.5 directly. The wavenumber where the weighted spectrum peaks is defined as k_{max}, indicated by a dashed line in Figure 2.1.

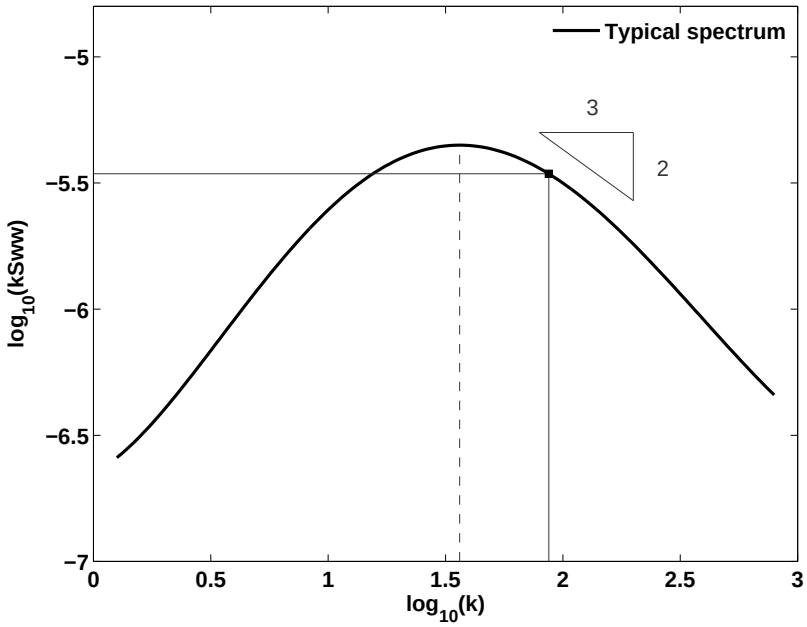

Figure 2.1: Typical weighted turbulence spectrum indicating the $-2/3$ relationship for k. The dashed line indicates k_{max}.

A fundamental turbulent length scale, the turbulent mixing length λ, characterises the size of the energy-containing eddies [McPhee, 2008a]. This is inversely proportional to k_{max} [McPhee and Morison, 2001], through

$$\lambda = \frac{0.85}{k_{max}}, \tag{2.2.6}$$

where the constant 0.85 is empirically determined [McPhee, 2004].

2.2.2 Turbulent kinetic energy

The turbulent energy in the ocean is generated in a variety of ways. Energy is supplied to turbulence through turbulent shear stress working against the mean shear of the flow [McPhee, 2008a], or by mechanically produced shear e.g. through interaction with topography [Padman, 1995]. In the Arctic Ocean a strong buoyancy forcing can drive turbulence through modifications of salinity and temperature, especially in the surface layer [Padman, 1995]. The full turbulent kinetic energy (TKE) equation can be reduced under the assumptions that the flow is steadily homogeneous and no mean vertical motion exists, together with no divergence of vertical flux [McPhee, 2008a]. Then usually three terms dominate the contribution to the TKE budget, and the rate of

change of energy is sustained or decaying due to their balance [Thorpe, 2007]. The simplified balance of TKE can be expressed as

$$\frac{dE}{dt} = P_S + P_B - \epsilon, \tag{2.2.7}$$

where $\frac{dE}{dt}$ is the rate of change of TKE with time, P_S is production by the mean flow due to shear, P_B is buoyancy production and ϵ is dissipation rate. P_S is always a positive term creating TKE, P_B changes sign with the surface forcing and ϵ always leads to a loss of TKE. This equation is valid for averaging over a long period of time or a large volume. For steady conditions $\frac{dE}{dt}$ is zero, and hence the terms on the right hand side must balance.

P_S can be calculated from the friction velocity u_* and the typical turbulent length scale λ as

$$P_S = \frac{u_*^3}{\lambda}, \tag{2.2.8}$$

where u_* can be calculated from covariances of the deviatory velocity components as

$$u_* = \sqrt[1/4]{\langle u'w' \rangle^2 + \langle v'w' \rangle^2}. \tag{2.2.9}$$

P_B can be calculated as

$$P_B = -g(\alpha \langle w'T' \rangle + \beta \langle w'S' \rangle), \tag{2.2.10}$$

where g is the gravitational constant, α is the thermal expansion coefficient, β is the saline contraction coefficient and $\langle w'T' \rangle$ and $\langle w'S' \rangle$ are kinematic heat flux and salt flux respectively. The thermal expansion coefficient is small for sea water close to the freezing point, and temperature plays a minor role compared to salinity in modifying the density of the water [Notz, 2005]. Hence, the salt flux in the surface layer due to ice formation is the governing buoyancy forcing at the surface.

2.2.3 Heat and salt flux balances

An ice surface in thermal equilibrium with the atmosphere requires the heat fluxes in and out of it to be balanced due to energy conservation [Eicken, 2003]. This includes short- and longwave radiation, sensible and latent heat fluxes and the conductive heat flux through the ice. At the lower interface between water and ice the fluxes included in

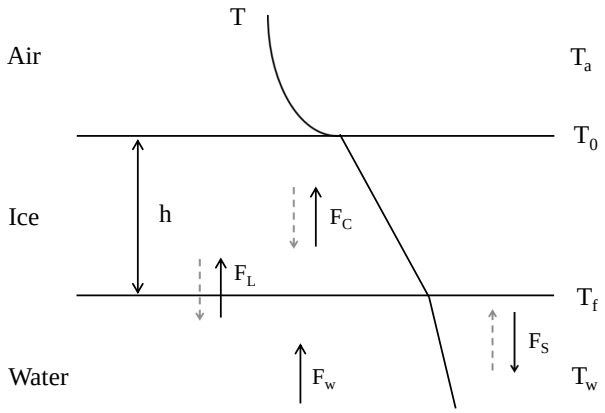

Figure 2.2: Flux balance at the lower interface of the ice. Black arrows indicate freezing, and grey arrows melting. F_L is latent heat flux, F_C is conductive heat flux, F_w is heat flux from the water and F_S is salt flux.

the energy balance are the latent heat flux F_L, the heat flux from the water F_w and the conductive heat flux F_C [Eicken, 2003], see Figure 2.2. F_L is the release of latent heat during freezing or uptake of heat during melting due to the change in ice thickness. F_C is the transfer of energy through the ice, due to the temperature gradient between the surface and the ice water interface. The energy balance at the lower interface can be expressed as

$$F_L = F_C - F_w. \tag{2.2.11}$$

As ice freezes at the ice-ocean interface salt will be released, and there will be a flux of salt into the ocean. When ice melts, the opposite will be the case and the salt flux will be directed towards the ice.

When the water is cooled or heated, fluxes of heat and salt modify the temperature and salinity of the water. Positive z-direction is defined upwards, giving positive flux direction toward the air or ice interface, and negative flux direction toward the bottom. The magnitude of F_w is dependent on the temperature difference between the water (T_w) and the air (T_a), whereas the direction is dependent on the sign of this temperature gradient. The salt flux is governed by a phase change, i.e freezing or melting of ice releasing saline brine or fresh water. The salt flux magnitude is decided by the amount of ice frozen or melted, and the direction on which of the two phase changes take place.

When $T_a < T_w$ (Figure 2.3a) the water cools and looses heat at the interface between water and air/ice, either to the atmosphere or to cooling or freezing ice and F_w is positive. When the water has reached the freezing point, formation of ice will start and

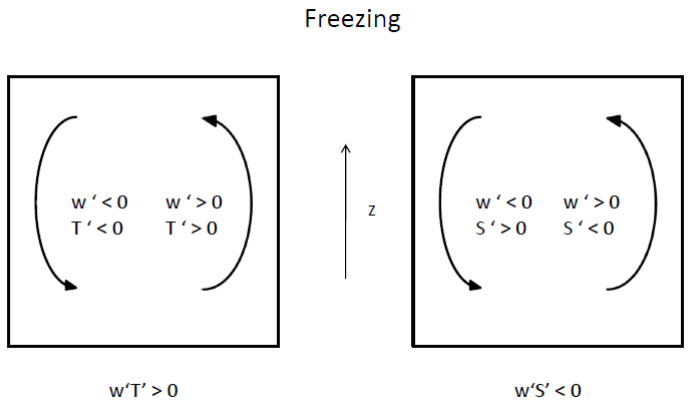

(a)

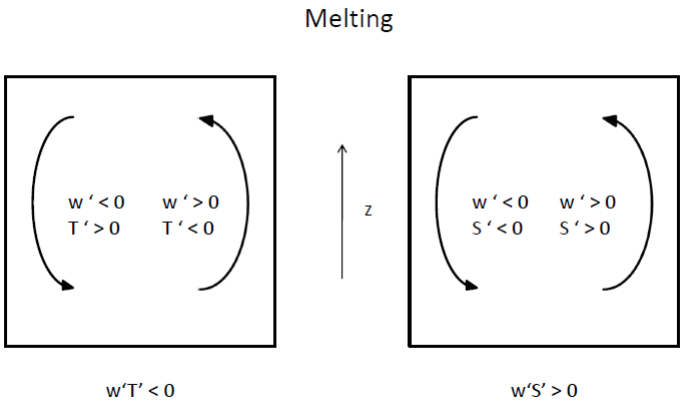

(b)

Figure 2.3: Turbulent heat flux (F_w) and salt flux (F_S) in the water during (a) freezing and (b) melting.

release of brine leads to a negative salt flux increasing the salinity of the water. In the opposite case, when $T_a > T_w$ (Figure 2.3b), the water gains heat from its surroundings and F_w is negative. As the water becomes warmer the ice will start melting and fresh water will be mixed down and decrease the salinity. This is defined as a positive salt flux.

2.2.4 Convective fluxes

In the case of no current during freezing, a convective system governs the turbulence due to the cooling at the surface. Plumes of water can form at the surface and periodically transport the cold and dense water into the interior, leading to a change in the density structure of the layer [Thorpe, 2007]. Assuming steady conditions and negligible P_S,

equation 2.2.7 will be reduced to a balance between P_B and ϵ [Thorpe, 2007].

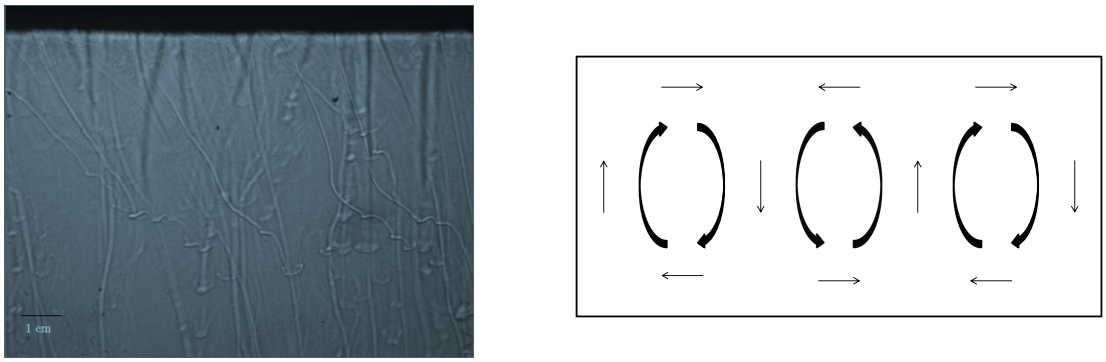

(a) **(b)**

Figure 2.4: (a) Shadow-graph photo of brine plumes in the water beneath ice grown from NaCl. The black area in the top of the picture is the ice (from Notz [2005]). (b) Schematic of a convective layer with three convection cells.

Figure 2.4a shows a picture from Notz [2005] of brine plumes leaving the ice. To conserve volume there must be a ascending fluid between the plumes [Thorpe, 2007], which Kelley [1990] assumes is supplied through horizontal movement along the horizontal boundaries, though not shown through laboratory measurements. This can be presented schematically as in figure 2.4b.

During melting the buoyancy forcing at the surface is stabilising, with warmer fresher water on top of saltier and colder water, and hence no plumes are expected to leave the surface.

3

Method

In this chapter, Section 3.1 contains an overview over how the experiments were conducted and the different setups used. Section 3.2 explains four different techniques used to calculate heat and salt fluxes in the tank, before the description of the procedure for finding brine plumes is presented in Section 3.3.

3.1 Experiments

The experiments were performed in a rectangular tank with a bottom area of 66 cm $\times$ 194 cm placed in an ice laboratory. The water was a NaCl solution of 34 kg salt added in approximately 90 cm deep fresh water, giving an initial salinity of 29 g/kg. This relatively low salinity was close to the one of surface water in the Arctic ocean of 30-32 g/kg [Wadhams, 2000]. The ice laboratory had a cooling ability of temperatures down to -25 °C, but the coldest temperatures used was -20 °C. Three different main setups of motion in the tank were used to study turbulence in the under-ice boundary layer and physical processes of sea ice growth in open water; circular current, stagnant water and standing wave. From the conducted experiments only circular current and stagnant experiments were further investigated in this study.

3.1.1 Instrumentation

Turbulence Instrument Cluster

Turbulence Instrument Cluster (TIC) is a cluster of sensors measuring turbulent heat, salt and momentum fluxes in the ocean boundary layer [McPhee, 2008a]. The system used in these experiments consisted of Sea-Bird Electronics sensors for temperature (T, SBE 3), conductivity (C, SBE 4), microConductivity (μC, SBE 7) and pressure (P, SBE 50) in combination with two 3-D ADV acoustic current meters (ADV1 and ADV2) from Sontek, all sampling at the same frequency (Figure 3.1a). The sampling frequency was 4 Hz for the current experiments, and 2 Hz for stagnant experiments. The ADV sensors consist of an acoustic sensor head with three receivers and one transmitter, and a temperature sensor. The velocity measurements were sampled in a small volume of 2 cm^3, 18 cm above the acoustic transmitter.

The reason for using two conductivity sensors was that typical salinity spectra show a developed inertial subrange [McPhee and Stanton, 1996], which can not be adequately resolved by the standard C sensor. The ducted and more accurate standard C sensor has a longer response time than the fast response μC sensor, which measures the conductivity of sea water by use of electrodes exposed directly to the water. The C sensor was used to calibrate the μC sensor, see more in appendix A.1. McPhee and Stanton [1996] found that the C sensor underestimates the salt flux by 25 % and by using the μC sensor more reliable estimates of the turbulent salt flux $\langle w'S' \rangle$ could be obtained.

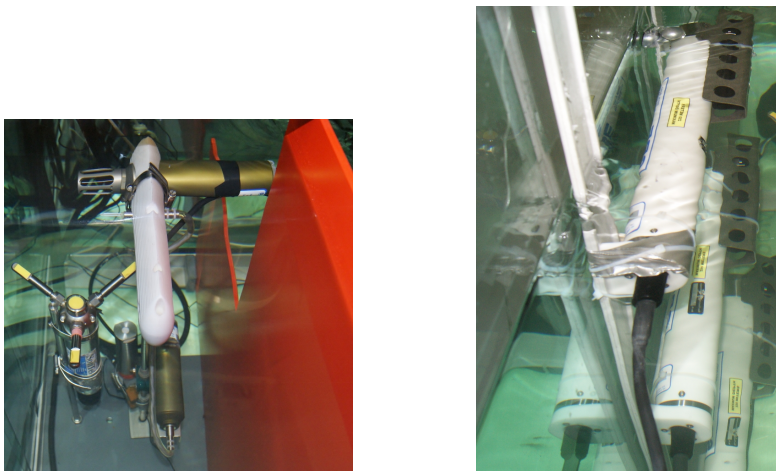

(a) **(b)**

Figure 3.1: Pictures of instrumentation: (a) TIC and (b) CTDs mounted on the side wall.

Other instruments

Four Seabird CTDs (SBE 37) (Figure 3.1b) were attached to the side wall at the depth of 8 cm, 44 cm, 71 cm and 85 cm during current experiments and at the depth of 8 cm, 32 cm, 62 cm and 85 cm during stagnant experiments. The CTDs were mounted horizontally due to the expected horizontal water movement from the current and wind during current experiments, and vertically during stagnant experiments when the water motion in the tank was expected to be vertical due to convection. A 22.5 cm long string with 29 thermistors was attached in the tank with approximately 2.5 cm in the air and the remaining 20 cm in the water, sampling every 7 seconds throughout all experiments. The CTDs sampled every 30 seconds during current experiments and every 10 seconds during stagnant experiments. Two wind sensors were placed above the water surface, together with a temperature and a humidity sensor.

3.1.2 Tank layout

Both freezing and melting experiments were performed with a bottom heat flux (F_b) provided by a heating wire at the bottom, with fluxes ranging from 0 Wm^{-2} to 31 Wm^{-2}. Typically 17 Wm^{-2} was used, but experiments with other values were also conducted. This high value was used to avoid crystals freezing at the instruments and disturbing the measurements. The walls of the tank were covered by 5 cm thick styrofoam to insulate them from the air, and make sure that the water was cooled mainly through the surface. The side walls were slightly heated with a 23 cm wide heating plate in the height of the surface, to have free floating ice that could move with the current. This heating also worked as a release of pressure built in the tank due to ice growth. A web-camera was attached in the center of the tank, and captured a picture every minute during the experiments. Before all freezing experiments were started the water was well mixed by the pumps and cooled to approximately 0.2 °C above the freezing point T_f . The melting experiments were all started directly after the freezing period ended.

During current experiments the ADVs sampled 71 cm above bottom, at the same height as the μC sensor and the T sensor. The C sensor and P sensor measured 24 cm above bottom (Figure 3.2a). ADV2 was placed 43 cm upstream of ADV1. The velocity measurements from ADV1 were made in a horizontal distance of 3 cm from the T and μC measurements in cross-stream direction, and 2.5 cm and 1 cm respectively in the along-stream direction. A pump, driving a clockwise current, induced maximal

velocities at 16 cm depth. The pump was heated with a wire to prevent frazil crystals freezing on it and disturbing the current. The wind was induced by an air hose attached to two connected pipes with small holes blowing in the same direction as the current at two places. The thermistorstring was attached to a division wall in the middle of the tank. During stagnant experiments the setup was changed (Figure 3.2b), but the distances between the sensors were approximately the same. The thermistorstring was no longer placed in the middle of the tank since the division wall was removed, but attached to the side wall.

3.1.3 Experiment setup

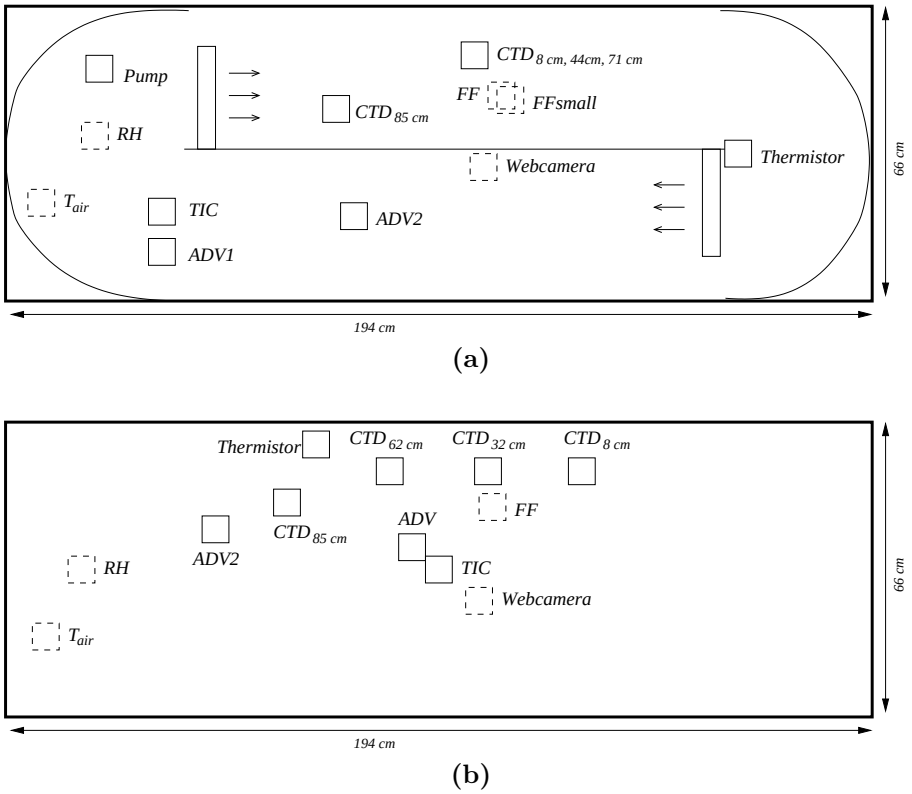

Figure 3.2: Horizontal overview of the experiment set up with (a) current and (b) stagnant water. Squares indicate the positions of the different sensors. Dashed squares are sensors in the air. In (a) the mid-line represents the division wall and the arrows the wind direction. Sketches are to scale.

Between the different classes of experiments the instrument setup was changed, see Figure 3.2a and Figure 3.2b for the plan view, and Figure 3.3a and Figure 3.3b for the vertical view. Two different main setups were used for the motion in the tank.

1. Current and wind made the water circulate clockwise around a division plate in the middle of the tank. The division plate was set up in a way that the water path was 33 cm wide and 30 cm deep. The short ends of the tank were made circular by a plastic wall for a smoother flow.

2. No motion. A ruler was attached to the side wall to measure ice thickness.

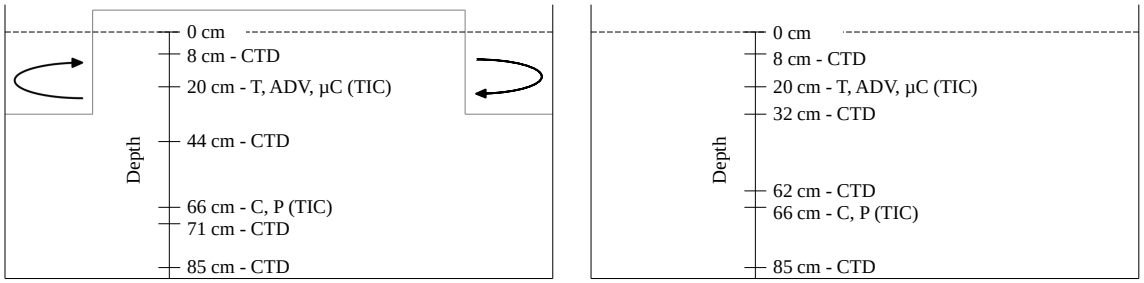

(a) **(b)**

Figure 3.3: Vertical setup during (a) current experiments and (b) stagnant experiments. In (a) the division wall is drawn from a side view. The arrows represent the clockwise current.

During the four-week experiment period, 26 experiments were performed. From these, 8 experiments were chosen to be further investigated; four from the circular current experiments (12, 13, 16 and 17) and four from the stagnant experiments (32, 33, 36 and 37). They were chosen as two pairs of freezing and melting experiments from the current setup and two pairs from the stagnant setup. They are listed in Table 3.1 with some key characteristics.

Exp	T_a	Duration	Motion	F_b
12	-15°C	24 h 25 min	Current and wind	17 Wm^{-2}
13	+5°C	25 h 15 min	Current and wind	17 Wm^{-2}
16	-15°C	8 h 50 min	Current and strong wind	17 Wm^{-2}
17	+5°C	8 h 50 min	Current and strong wind	17 Wm^{-2}
32	-15°C	8 h 25 min	Stagnant	31 Wm^{-2}
33	+5°C	13 h 20 min	Stagnant	31 Wm^{-2}
36	-15°C	23 h 5 min	Stagnant	17 Wm^{-2}
37	+5°C	23 h 20 min	Stagnant	17 Wm^{-2}

Table 3.1: Overview of analysed experiments.

The data used was mainly from the TIC and the CTDs, together with the manual

ice thickness measurements and thermistorstring data. Unless otherwise stated, the velocity measurements were from ADV1. During the current experiments ice samples were taken to analyse the ice and its properties, see more in Naumann [2011]. The initial salinity for each experiment was not the same due to ice sampling and evaporation, and one should be careful comparing absolute numbers. In addition the conversion from conductivity to salinity was done with equations for seawater. NaCl is the main salt constituent of sea water [Kester et al., 1967], but it is not straight forward that the conversion is exactly similar. See more in A.2. The cooling room had a defrosting period of approximately half an hour every sixth hour. This gives visible temperature changes, especially in the thermistor string data. An overview of all conducted experiments is listed in Table B.1.

3.2 Flux estimation techniques

The heat and salt fluxes in the tank were calculated by four different techniques; heat and salt content, covariance, residual and spectral method. The heat flux was calculated by all four methods and the salt flux by salt content, covariance and spectral method. These methods will be presented in this section.

3.2.1 Heat and salt content method

Vertical fluxes were estimated from observed mean values of T and S from all sensors and their changes with time. These fluxes will be used as a basis for comparison with the other methods, since the observed changes has to represent the fluxes present. The heat flux by this method was found for each 10 minute time step as

$$F_w = -\rho_w c_p d \frac{dT_w}{dt} + F_b, \tag{3.2.1}$$

where ρ_w was the water density, c_p was the specific heat capacity of water and d was the water depth. $\frac{dT_w}{dt}$ was the vertically averaged temperature change in the tank during each 10 minute timestep and F_b was the bottom heat flux. Equation (3.2.1) gave the heat flux required to fit the observed temperature changes. The negative sign made sure that the direction of the flux was correct.

In the same way the salt flux can be calculated as

$$F_S = -d\frac{dS}{dt}, \tag{3.2.2}$$

where $\frac{dS}{dt}$ was the vertically averaged change in salinity in the tank during each 10 minute timestep. The negative sign again made sure that the flux direction was correct.

The heat and salt fluxes calculated by this method will be referred to as content heat flux and content salt flux throughout this thesis.

3.2.2 Covariance method

The turbulent salt and heat fluxes were estimated by the covariance method, where the mean of the covariance of the fluctuating parameters was evaluated. The turbulent time series were calculated by subtracting the mean values from the original values over an averaging period short enough to retain the trend, but long enough to reduce signal noise, here chosen to be 10 minutes. The turbulent heat flux in Wm^{-2} can be expressed by the covariance method as

$$F_w = \rho_w c_p \langle w'T' \rangle, \tag{3.2.3}$$

where ρ_w is water density and c_p is the specific heat capacity. $\langle w'T' \rangle$ is the mean covariance of the fluctuations of vertical velocity and temperature.

Similarly the turbulent salt flux can be calculated as

$$F_S = \langle w'S' \rangle, \tag{3.2.4}$$

where $\langle w'S' \rangle$ is the turbulent deviations of vertical velocity and salinity from the mean.

When using the covariance method the turbulence field was assumed to be isotropic and Taylors's hypothesis was applicable. Taylor's hypothesis assumes that the turbulence field is considered frozen as it is advected past a sensor (e.g. Stull [2008]). This is useful for cases when evolving an eddy takes longer than the time it takes for one eddy to pass the sensor.

In the stagnant experiments there was little horizontal movement. The buoyancy forcing was expected to control the vertical movement through convection (Figure 2.4), and since the fluxes were calculated from the deviations in vertical velocity the

covariance method was assumed valid also in stagnant experiments.

3.2.3 Residual method

By using a residual method, the ocean heat flux could be calculated assuming that all heat lost/gained in the water was the difference between heat conducted through the ice (F_C) and latent heat used to melt/freeze ice at the ice water interface (F_L) [Eicken, 2003]. This was expressed by equation 2.2.11, where F_C and F_L were

$$F_C = \frac{k_i(T_f - T_0)}{h} \tag{3.2.5a}$$

$$F_L = \rho_i \frac{dh}{dt} L(\phi). \tag{3.2.5b}$$

k_i was the thermal conductivity, T_f and T_0 were the freezing and surface temperature respectively, h was the ice thickness, ρ_i was the ice density, t was time and L was the latent heat of fusion dependent on solid fraction. F_C would go to infinity as the ice thickness decreased to zero. Therefore the ice thickness was limited to be at least 1 mm when ice was present, and further F_C was omitted for smaller ice thickness or no ice.

3.2.4 Spectral method

As a fourth method, the heat flux was estimated using a spectral technique described by McPhee [2004]. This method was applicable where the turbulence was well developed and a typical turbulent mixing scale existed. It also assumed that buoyancy forces were negligible.

The function *pwelch* in MatLab was used to find the power spectral density (PSD) of the deviatory time series of vertical velocity and temperature. The spectrum was transformed from frequency to wavenumber, and weighted wavenumber spectrum of vertical velocity ($\phi_w = kS_{ww}(k)$) and temperature ($\phi_T = kS_{TT}(k)$) were calculated for each 10 minute interval. The weighted spectra have units of velocity squared, and were smoothed into equally spaced bins of *log* k with length 0.2. Each of the 10 minute binned spectra were fitted with a fifth order polynomial, and the wavenumber for maximum energy k_{max} was identified by the peak of the polynomial fit. Values for corresponding binned wavenumber and the polynomial fit were used to find a spectral value for vertical velocity and temperature, ϕ_w and ϕ_T, evaluated for a wavenumber in

the inertial subrange where the slope in log-log space was -2/3. Dimensional analysis suggested a relation between the weighted spectrum and the friction velocity to find a normalised spectrum $\Phi(k/k_{max})$,

$$\frac{\phi_w}{{u_*}^2} = \Phi_w(k/k_{max}). \tag{3.2.6}$$

To find an estimate of the turbulent heat flux magnitude the velocity spectrum was combined with the temperature variance spectrum. The nondimensional spectra of temperature and vertical velocity could be calculated through equations (3.2.7) and (3.2.8), where $c_\gamma = 0.48$ and $c_T = 0.83$ were constants [McPhee, 2004], and k_{max} was known from the peak of the polynomial fit,

$$\Phi_w(k) = c_\gamma(\frac{k}{k_{max}})^{-(2/3)} \tag{3.2.7}$$

$$\Phi_T(k) = c_T - \frac{4}{3}(\frac{k}{k_{max}}). \tag{3.2.8}$$

From dimension analysis a nondimensional relation for the combined temperature and velocity spectrum was given as

$$\frac{\phi_w \phi_T}{\overline{w'T'}^2} = \Phi_T. \tag{3.2.9}$$

The kinematic heat flux was calculated by equation (3.2.10), following from equation (3.2.9),

$$log|\overline{w'T'}| = \frac{1}{2}(log\phi_w + log\phi_T - log\Phi_T). \tag{3.2.10}$$

This technique was also expanded to calculating salt fluxes. In an analogue way the kinematic salt flux magnitude could be expressed as

$$log|\overline{w'S'}| = \frac{1}{2}(log\phi_w + log\phi_S - log\Phi_S). \tag{3.2.11}$$

It was then assumed that in a turbulent flow scalar properties such as temperature and salinity were exchanged at the same rates, hence same constants for c_γ and c_T could be used.

3.3 Brine plume detection

Measurements have shown that dense brine is released to the ocean underneath sea ice in convective events, both during freezing conditions [McPhee and Stanton, 1996] and in situations where heat budget evaluations at the ice-water interface suggests melting [Widell et al., 2006]. These intermittent convective events released from sea ice, called brine plumes, drain the brine out of the ice. Plumes of saline and cold water causes a negative salt flux strongly correlated with a positive heat flux to the ice.

Brine plumes detected during the experiments were characterized by $w' < 0$, $S' > 0$ and $|\langle w'S' \rangle|$ greater than the root mean square (rms) value for the whole record. To ensure that the plume signal was not only spikes in the dataset the requirements had to be fulfilled for at least 3 seconds. Widell et al. [2006] used $|\langle w'S' \rangle|$ greater than five times the rms value to detect plumes leaving fast ice of thickness $\sim$ 1.2 m. This was too strict for the brine plumes emanating from thin ice of only a few centimetres.

The rms value was calculated as

$$rms_{(w'S')} = \sqrt{\frac{w'S'_1 + w'S'_2 + ... + w'S'_n}{n}}, \tag{3.3.1}$$

where n was the number of measurements in each experiment. Because of high background turbulence in the tank the rms value was one order of magnitude larger for the current experiments compared to the stagnant experiments. The center of the plumes were chosen to be in the middle of each detected plume signal. The mean structure of the brine plumes released from the ice was found by averaging over all detected events during each experiment in a similar way as Widell et al. [2006].

The importance of the salt and heat fluxes during brine plumes was calculated as a percentage of the mean content salt and heat flux. In current experiments the salt and heat fluxes from the plumes during freezing were expected to have the same sign as the general fluxes in the tank, and enhancing them. During melting the plume fluxes were expected to be of opposite sign of the overall fluxes, and hence counteracting the heating and freshening of the water in the tank.

4

Results

This chapter contains a presentation of the results from the experiments. It is separated into a general description of the temperature and salinity development in Section 4.1, before the results from the TKE evaluation are presented in Section 4.2. In Section 4.3 the results from the different flux estimation techniques are presented, and thereafter the results considering the brine plumes in Section 4.4.

4.1 Temperature and salinity development

In this section contourplots of temperature and salinity development with time for the whole depth from the four CTDs and the TIC are presented. The data was interpolated in 10 cm vertical distance, and onto the TIC time stamp of 10 minute intervals. In addition the dataset was extrapolated to the surface, which will, especially during stagnant experiments, possibly give misleading surface temperatures. Thermistorstring data is presented with the same temporal resolution of 10 minute intervals, but with a higher vertical resolution with 28 sensors within 22.5 cm.

The TIC salinity was corrected during current experiments, since it clearly had an offset compared to three of the CTDs. The top CTD was not included in the correction calculations, since it also deviated from the three other CTDs. When the water was well mixed the TIC salinity showed values $\sim$ 0.36 g/kg lower than the CTDs, which were measuring similar values. A value of 0.36 g/kg was therefore added to the TIC salinity. This was not clear during stagnant experiments, and no correction was made.

4.1.1 Current experiments

The experiments started while the water was well mixed, and had a temperature of approximately -1.6 °C. Typically the freezing of ice started 1-2 hours into the experiment, when the water was slightly supercooled, and small frazil crystals with diameter 2 - 3 mm formed. Due to the turbulence they were floating with the current and suspended in the top centimetres forming a grease ice layer. The crystals soon accumulated in the short ends of the tank, and the grease layer had a thickness up to 20 cm before it consolidated. The ice then grew towards the middle of the tank from the sides, see figure 4.1a, with some open water remaining where the wind was strongest. Approximately 5 hours after initial ice formation the surface was covered by an inhomogeneous ice layer, with thickness varying with several centimetres. During melting the wind efficiently distributed the warm air and blew it against the ice surface, leading to surface melting.

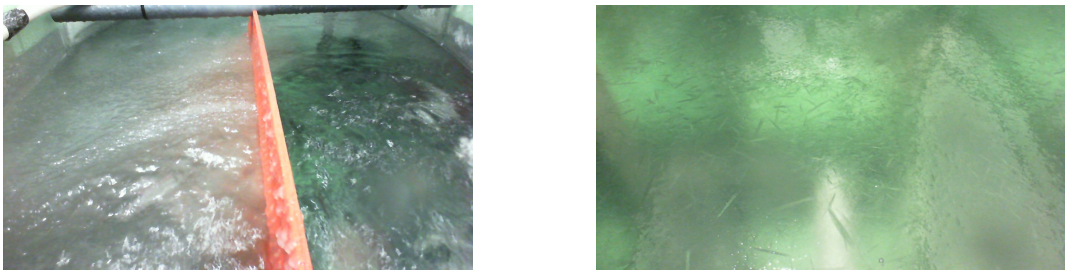

(a) **(b)**

Figure 4.1: Pictures of ice freezing during (a) current experiment 16 and (b) stagnant experiment 32.

Temperature

The water was still cooling the first hour of the freezing experiments throughout the water column, and reached values of -1.76 °C and -1.79 °C during experiment 12 and 16, respectively, before ice crystals started forming (Figure 4.2a). The temperature was uniform and there was no pronounced signal from the bottom heat flux (Figure 4.3a and 4.3c), indicating that the water was well mixed. The temperature increased after onset of freezing with 0.04 °C during experiment 12 and 0.13 °C during experiment 16.

After the temperature in the room changed from freezing to melting conditions the temperature increased in the water, first slowly as the ice melted, and faster when the ice was gone (Figure 4.2a, exp 13). Meltponds immediately appeared at the surface due

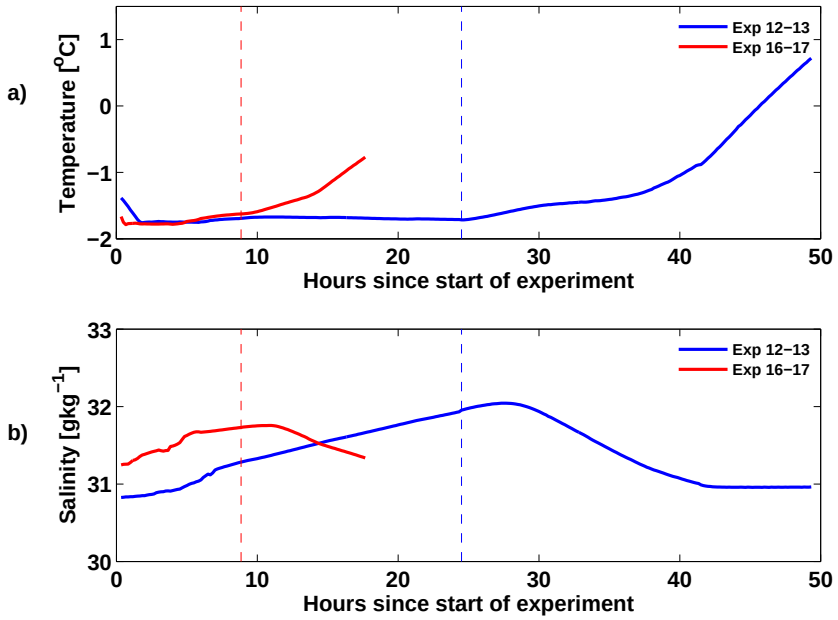

Figure 4.2: a) Vertically averaged temperature and b) salinity development during current experiments. Dashed lines mark the change from freezing to melting experiment.

to the wind distributing the warm air, and the low-salinity surface ice started to melt from above. The ice cover opened up after approximately five hours, and turbulence efficiently increased the exchange of heat, leading to a further warming of the water. After 17 hours of melting during experiment 13 all ice was gone, but the water still had a temperature of -0.6 °C. This indicated that the solid ice was melted from above and/or dissolved by the saline water at the ice-water interface.

Salinity

As ice started freezing the salinity increased in the whole water column, which continued to be well mixed due to the current (Figure 4.3b and 4.3d). The salinity increased with 1.12 g/kg during experiment 12, and 0.48 g/kg during experiment 16. After onset of melting, the salinity increased with 0.03 g/kg h^{-1} the first three hours of experiment 13 to a peak value of 32.04 g/kg, and 0.01 g/kg h^{-1} the first two hours of experiment 17 to a peak value of 31.76 g/kg (Figure 4.2b). In experiment 13 the strongest salinity signal was in the lower part of the water column. After reaching the maximum value, the salinity again decreased as the solid ice matrix was dissolved and the surface opened up and the mixing was more efficient. Towards the end of the melting period the salinity

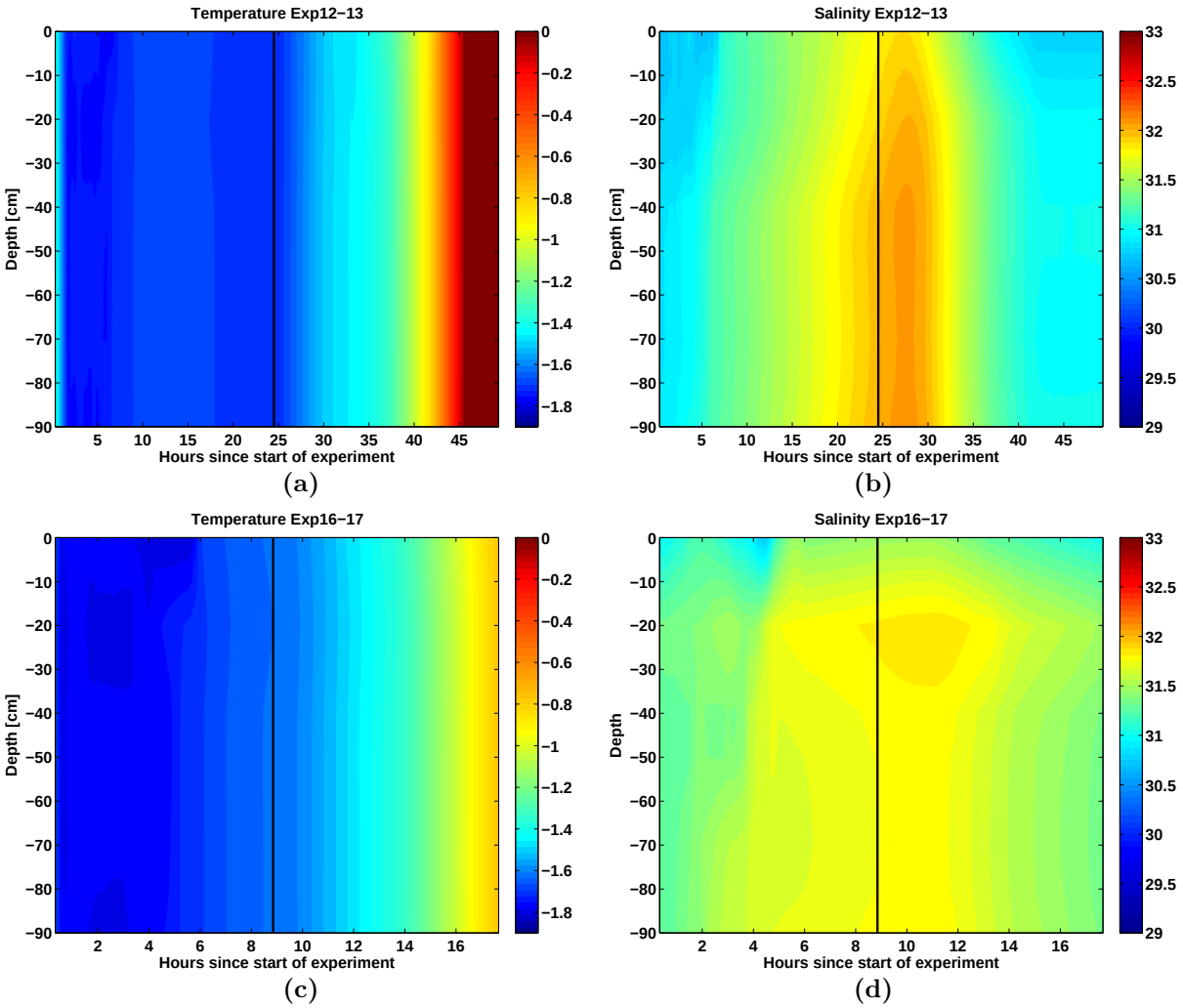

Figure 4.3: (a) Temperature and (b) salinity development during experiment 12 and 13. (c) Temperature and (d) salinity development during experiment 16 and 17. Solid vertical line indicates the change from freezing to melting experiment.

in the top layer decreased. The salinity towards the end of experiment 13, after all ice has melted, was 0.14 g/kg higher than at the beginning of experiment 12 (Figure 4.2b). This was due to some evaporation and ice sampling during the experiments. At the end of experiment 17 all ice had not melted.

Surface layer temperature

Throughout the freezing periods the temperature in the top layer decreased due to the cold air temperature (Figure 4.4a and 4.4c). The first few hours the air closest to the surface was strongly affected by the heat in the water, and remained relatively warm compared to the overall temperature in the room. There was a strong temperature

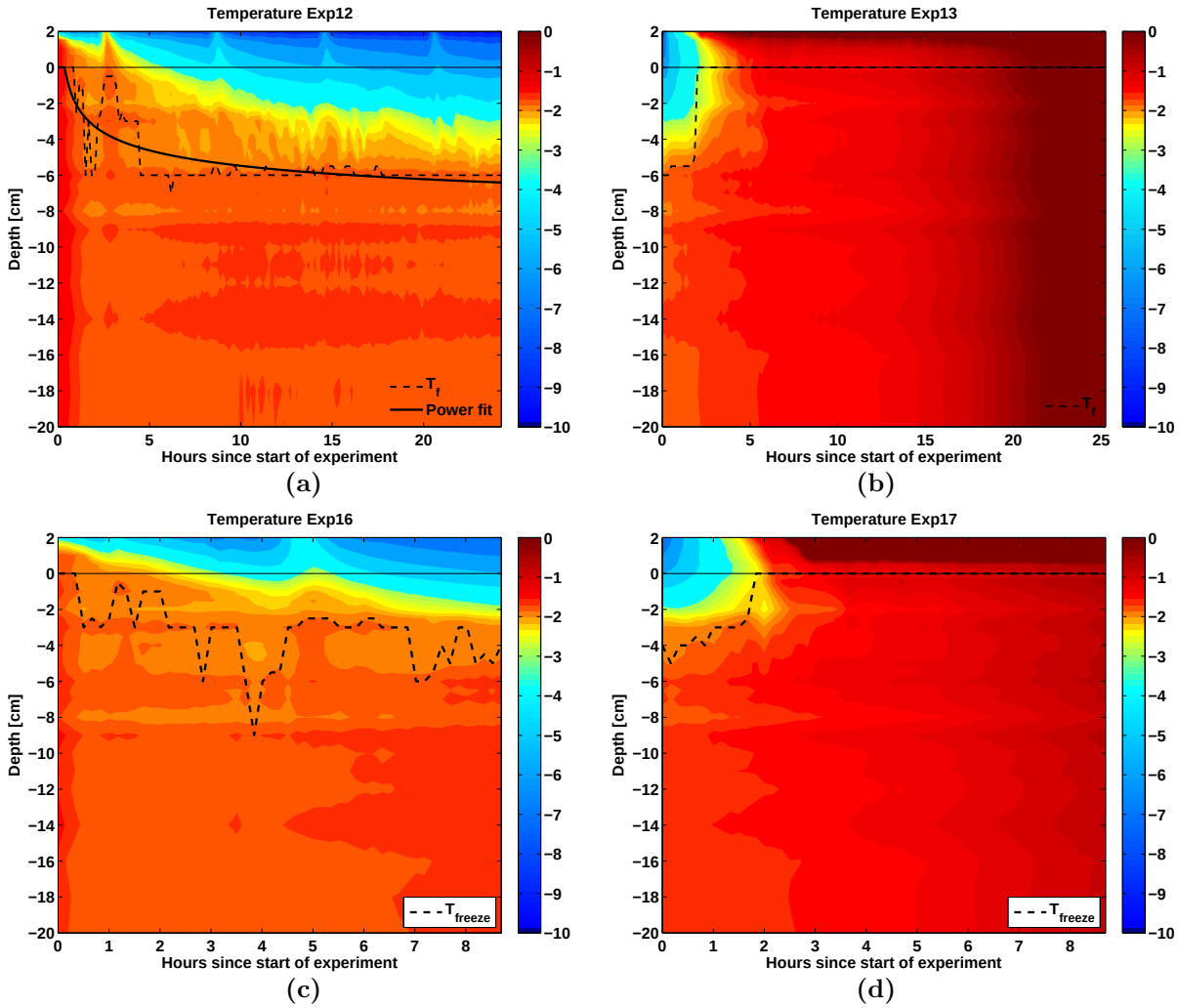

Figure 4.4: Temperature development from thermistorstring data for (a) experiment 12, (b) experiment 13, (c) experiment 16 and (d) experiment 17. The dashed line represented the depth of T_f calculated from the top CTD and the solid line was an approximation to this. Horizontal line indicates interface between surface and air.

gradient in the area of the interface between ice and water. To get an approximation of the ice thickness, the freezing point T_f (Figure 4.4a and 4.4c, dashed line) was calculated with the top CTD salinity through equation A.3.1. The temperature at the interface between water and ice always had to be at the freezing point, and the highest position T_f had in the water column would then be an approximation to ice thickness. This approximation changed vertically up and down the first hours of experiment 12, but when the ice was consolidated after approximately 5 hours the depth was close to constant at 6 cm. T_f was shallower for experiment 16 than experiment 12, and did not reach a constant depth. The solid line was a fit to the ice thickness approximation, represented by an equation on the form $h = at^b + c$ where t was time and a, b and

c were constants. This form for the approximation was chosen since ice is expected to grow with square root of time according to Stefan's law [Leppäranta, 1993]. The defrosting period of the cooling room was visible every sixth hour as an increase in temperature of the air and top centimetres of ice/water.

As the room temperature was turned to +5°C the water temperature increased, first slowly then faster (Figure 4.4b and 4.4d). The gradients were smoothed out with time due to the increased mixing in the water by wind and current when the ice was melted.

4.1.2 Stagnant experiments

The water in the tank was mixed manually before start of the stagnant freezing experiments to make sure there was no stratification. The ice started freezing immediately after experiment start and a thin layer of approximately 1 mm was covering the surface after only 30 min (figure 4.1b). This occurred at a time when the vertically averaged temperature was 0.2 - 0.3 °C above T_f (Figure 4.5a). The ice thickness was homogeneous throughout the tank and measured by a frozen-in ruler. At the end of the melting periods the ice had not disappeared, and it was only slightly thinner than at the beginning of the melting period.

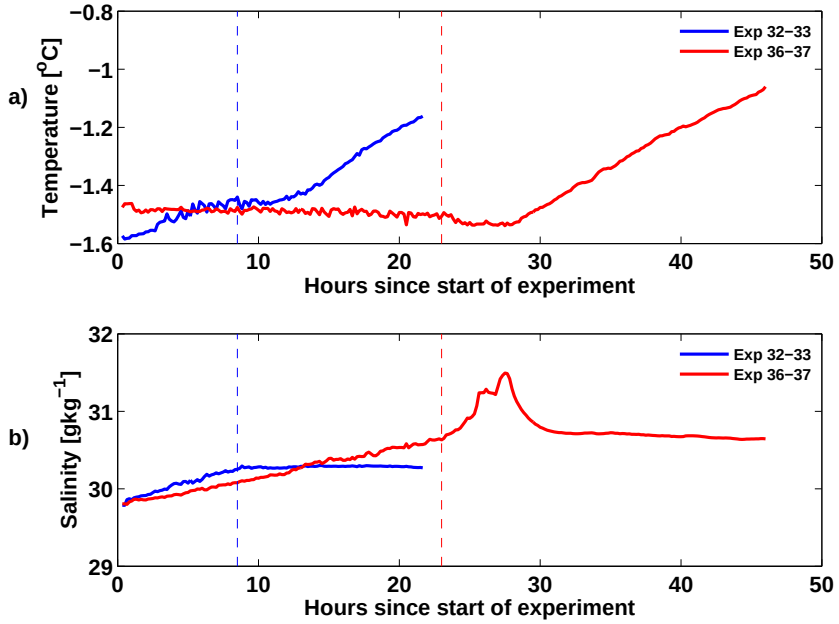

Figure 4.5: a) Vertically averaged temperature and b) salinity development during current experiments. Dashed lines mark the change from freezing to melting experiment.

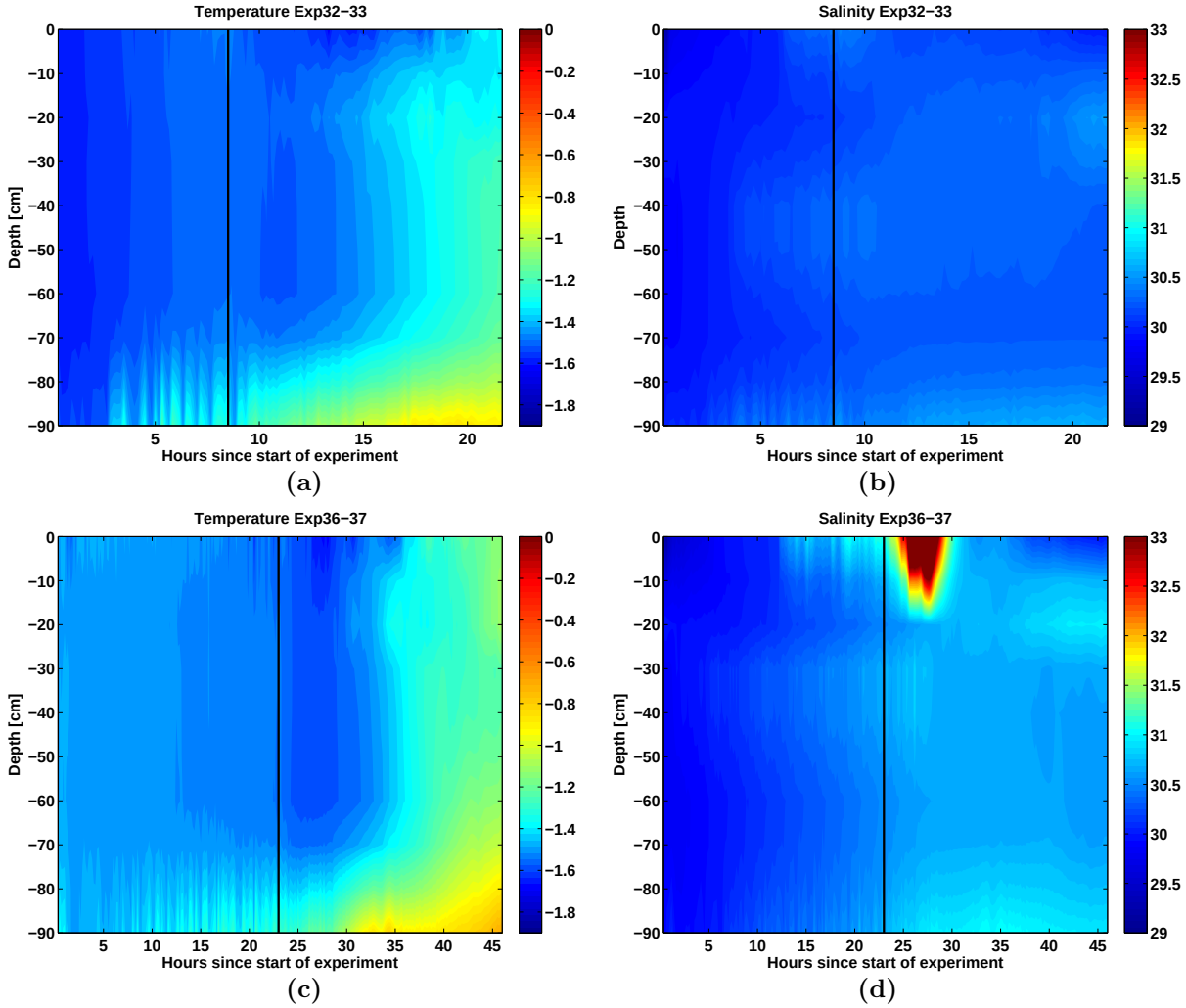

Figure 4.6: (a) Temperature and (b) salinity development during experiment 32 and 33. (c) Temperature and (d) salinity development during experiment 36 and 37 Solid vertical line indicates the change from freezing to melting experiment.

Temperature

The weak turbulence in the water allowed the heat flux input from the bottom to influence the temperature (Figure 4.6a and 4.6c), and by convection this heat mixed in. The overall temperature in the water column was higher than for the current experiments, indicating a strong stratification in the top centimetres. During experiment 32 the temperature increased by 0.13 °C, from -1.57 °C to -1.44 °C, and was well above T_f. Experiment 36 had a relatively constant temperature of -1.5 °C.

As the ice started melting the temperature first decreased slightly before it started increasing. The warming started from the bottom, and due to the stable salinity

stratification the water at the bottom was denser although warmer than at higher levels. The temperature in experiment 33 and experiment 37 were -1.16 °C and -1.06 °C at the end of the melting period respectively. When examining the ice after the experiments it was soft, mushy, had a low solid fraction and an ice thickness close to the one at the end of the corresponding freezing period.

Salinity

The salinity was steadily increasing during the freezing experiments (Figure 4.5b). In experiment 32 the salinity increased with 0.05 g/kg h^{-1} during 8.5 hours of freezing, and in experiment 36 the salinity increased with 0.04 g/kg h^{-1} during 23 hours of freezing.

After the melting started the salinity in experiment 33 did not change. In experiment 37 the salinity increased 0.87 g/kg during the first 4.5 hours of melting, and was strongly affected by the large increase in salinity in the top centimetres (Figure 4.6d). The difference to the current experiments was that the stratification was more stable and the saline water was at the bottom with less saline on top (Figure 4.6b and 4.6d). Towards the end of the melting period the salinity in the surface layer decreased slightly, and the solid ice released some freshwater through melting or dissolution. The increased salinity in the top layer the first few hours of melting in experiment 37 will be discussed in Section 5.4.

Surface layer temperature

As the ice started freezing immediately after the experiments started, the interaction between air and water was through the ice. The water was relatively warm close to the ice/water interface compared to T_f, and the stratification in temperature was strong (Figure 4.7a and 4.7c). The temperature increased by 1 °C over only 3 cm vertical distance e.g. in experiment 32. Again the dashed line represents the location of the freezing point temperature from the top CTD, and the solid line the fit to it. This was generally deeper than the measured ice thickness marked by asterisks (Figure 4.7a and 4.7c). The defrosting period every sixth hours was visible in the ice and air with an increase in temperature.

Even if the room temperature was +5 °C, the air just above the surface remained cold for approximately 4 hours before the gradient turned towards a heating of the water

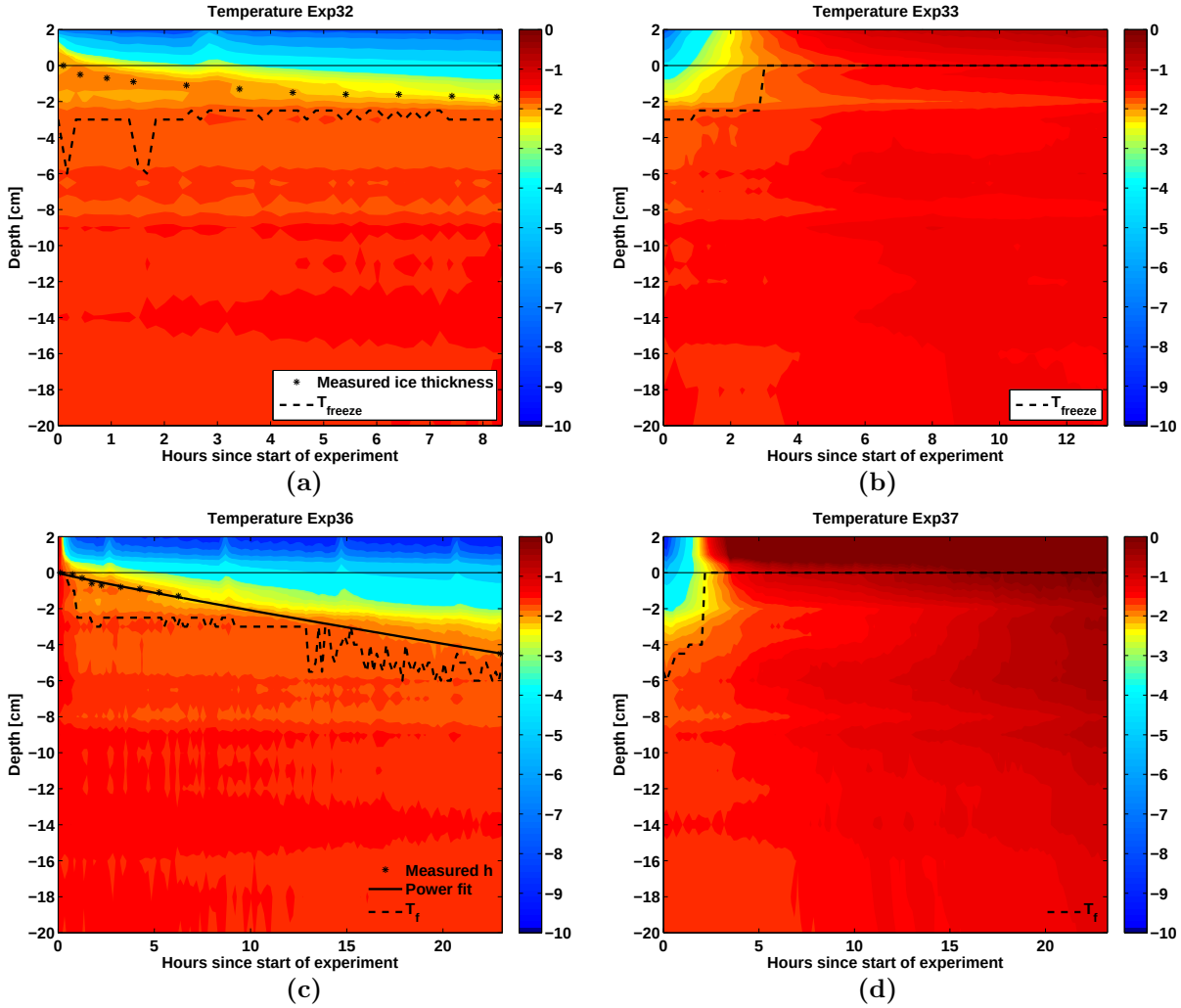

Figure 4.7: Temperature development from thermistorstring data for (a) experiment 32, (b) experiment 33, (c) experiment 36 and (d) experiment 37. The dashed line represents the depth of the freezing temperature calculated from the top CTD and the solid line is an approximation to this. Asterisks are measured ice thickness. Horizontal line indicates the interface between surface and air.

(Figure 4.7b and 4.7d). There was a stable stratification in the air with cold air close to the ice surface, leaving the surface temperatures close to 0 °C instead of +5 °C. This indicated that the only loss of ice thickness was due to dissolution of ice at the ice-ocean interface.

4.2 Turbulence measurements

The high frequency turbulence measurements from the TIC could typically look like the deviatory time series of temperature, salinity and velocity displayed in figure 4.8 for a 30 minute interval. The coordinate system was aligned so that the main current was in negative x-direction along the tank, y-direction across the tank and z-direction positive upwards. The time series were plotted as deviations from linearly detrended 10 minute intervals. This section will contain results from the turbulence measurements considering the turbulent kinetic energy balance and the typical mixing length λ.

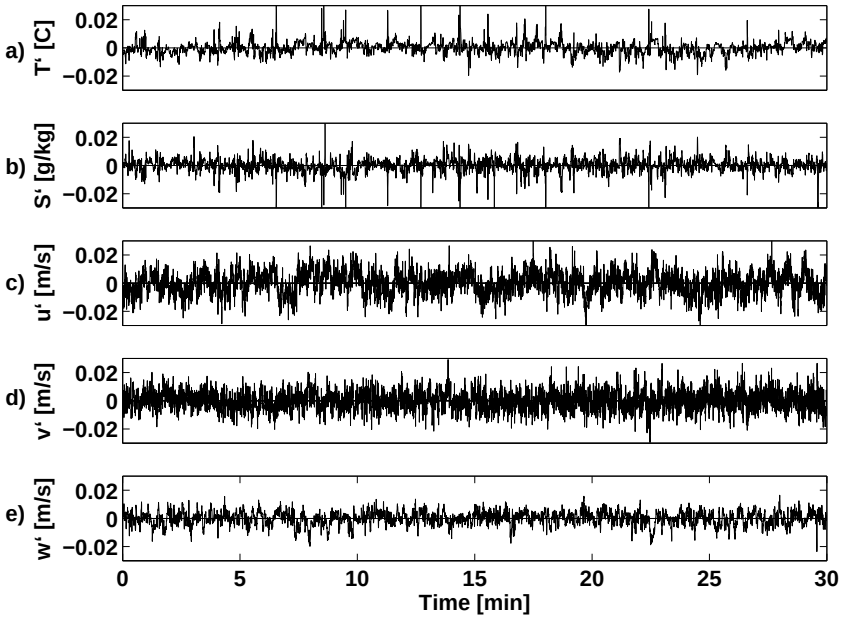

Figure 4.8: Deviatory time series of a) temperature with mean value -1.52 °C, b) salinity with mean value 30.4 g/kg, c) x-direction velocity with mean value -0.02 m s^{-1}, d) y-direction velocity with mean value -0.007 m s^{-1}, e) vertical velocity with mean value 0.0003 m s^{-1}. This was a record from experiment 12.

4.2.1 Turbulent kinetic energy

To calculate the power spectral density (PSD) and get useful results the turbulence needs to be well developed. Figure 4.9a shows a weighted turbulence spectrum from experiment 12 where the turbulence indeed was well developed and there was a lot of irregular movement in the water. The $k^{-2/3}$ dependency was visible in the weighted spectrum as a constant gradient at high wavenumbers, which could be used to calculate

the dissipationrate, ϵ. The spectra from ADV2 have similar shape as spectra from ADV1, but with a shift towards higher energies and lower wavenumbers.

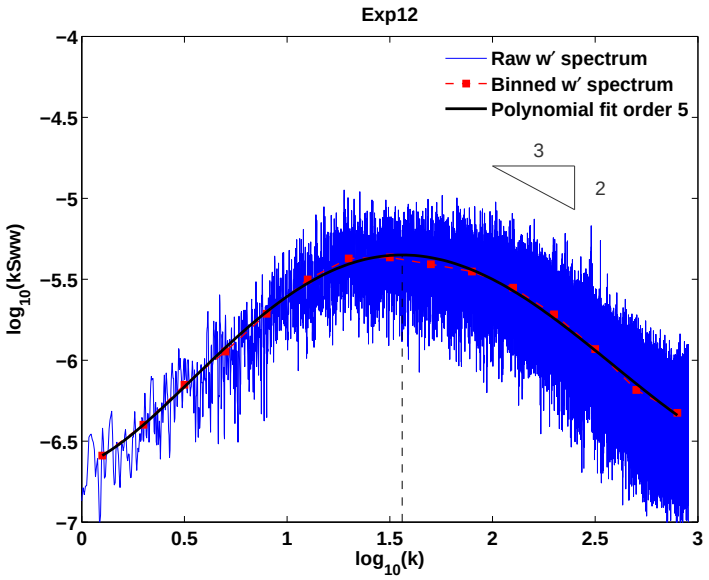

(a)

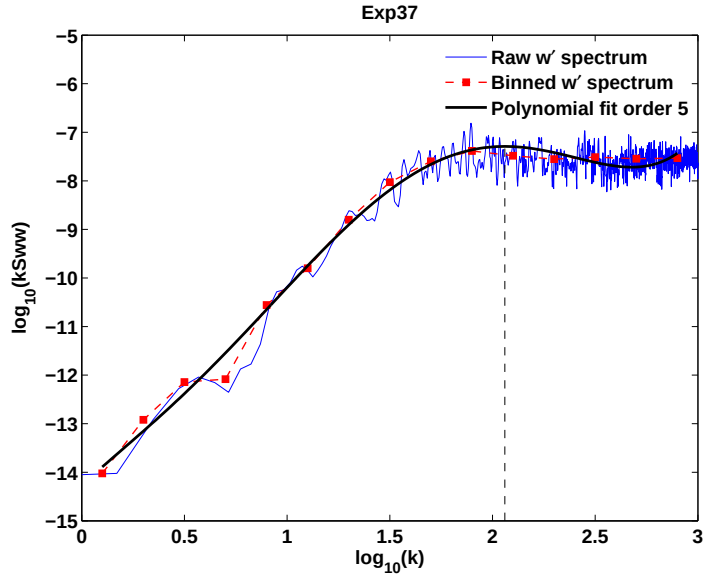

(b)

Figure 4.9: Weighted turbulence spectrum of vertical velocity during (a) experiment 12 and (b) experiment 37. Dashed line indicated k_{max}. The blue graph is the raw weighted PSD spectrum for w', red line the binned spectrum, and black line the polynomial fit to the binned spectrum.

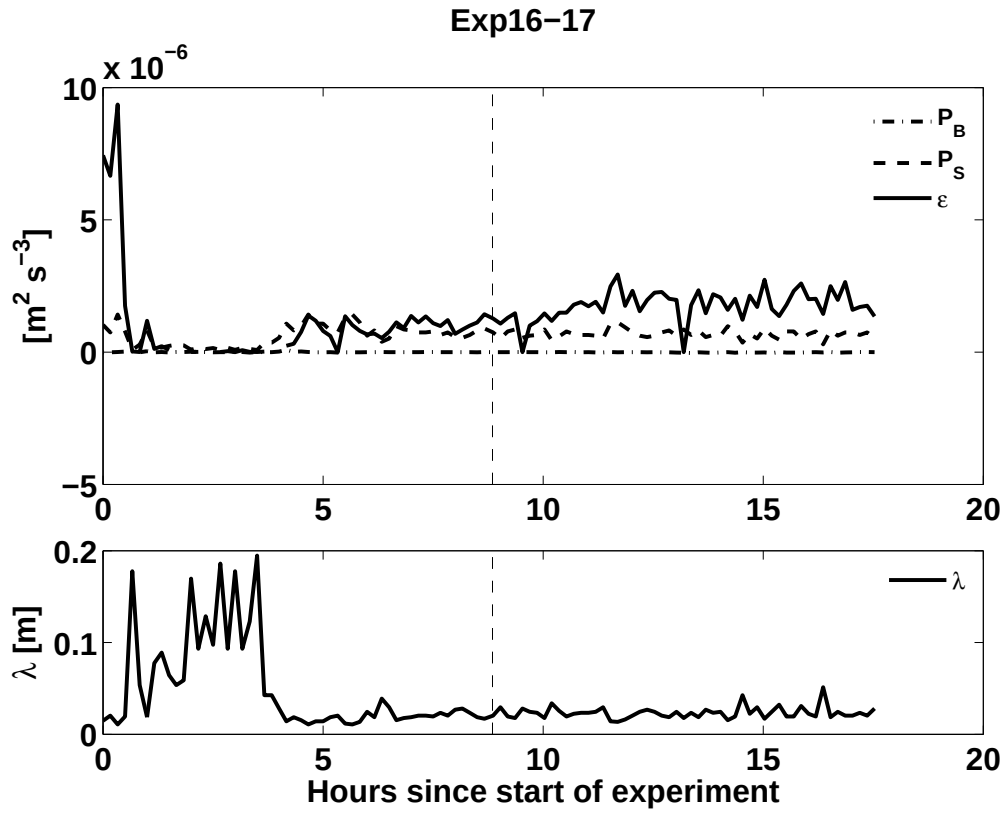

Figure 4.10: Development of the different terms in the TKE balance together with λ, presented as half an hour means. Dashed vertical line indicates change from experiment 16 to 17.

Figure 4.10 shows the development of the terms in the TKE balance with time during experiment 16 and 17. In the experiments with current the main contributor to turbulence was shear production, and buoyancy forcing could be assumed negligible. ϵ was largest during the start of experiment 16 and at the end of experiment 17, the times when the water was open. The shear production, P_S, stayed relatively constant throughout the experiments except the first hours of experiment 16 when it was smaller. Throughout the experiments P_S had lower values than ϵ. The buoyancy production, P_B, was two orders of magnitude smaller than the other terms, and no fluctuations could be seen from this figure. This resulted in a negative total TKE balance for large parts of the experiments. λ had largest values the first five hours of experiment 16 with values up to 0.2 m. Later it was fluctuating around values close to 0.02 - 0.03 m.

The mean values of the different terms in the TKE equation for the current experiments are presented in Table 4.1. The terms expected to dominate were P_S and ϵ, and by assuming steady state they should ideally cancel each other out. P_B was two orders of

magnitude smaller than both P_S and ϵ, as expected. The typical mixing length λ was larger at the site of ADV2 compared to the site of ADV1, with mean values of 0.06 m and 0.03 m respectively. ϵ decreased downstream from ADV2 and was approximately half its size at the site of ADV1. P_S showed similar values at both locations.

	ADV1				ADV2		
Exp	P_B	P_S	ϵ	λ	P_S	ϵ	λ
12	$1.33 \cdot 10^{-9}$	$0.73 \cdot 10^{-6}$	$1.21 \cdot 10^{-6}$	0.02	$0.37 \cdot 10^{-6}$	$2.78 \cdot 10^{-6}$	0.06
13	$-1.68 \cdot 10^{-9}$	$0.61 \cdot 10^{-6}$	$1.75 \cdot 10^{-6}$	0.03	$1.70 \cdot 10^{-6}$	$3.71 \cdot 10^{-6}$	0.06
16	$3.67 \cdot 10^{-9}$	$0.75 \cdot 10^{-6}$	$1.27 \cdot 10^{-6}$	0.04	$0.70 \cdot 10^{-6}$	$3.07 \cdot 10^{-6}$	0.05
17	$-7.39 \cdot 10^{-9}$	$0.53 \cdot 10^{-6}$	$1.48 \cdot 10^{-6}$	0.03	$0.90 \cdot 10^{-6}$	$3.10 \cdot 10^{-6}$	0.05

Table 4.1: Comparison of P_S $[m^2 s^{-3}]$, P_B $[m^2 s^{-3}]$, ϵ $[m^2 s^{-3}]$ and λ $[m]$ during current experiments, calculated from the two ADVs. Due to a lack of temperature and salinity measurements at the ADV2 site, P_B could not be calculated there.

The only turbulent forcing for movement during freezing in the stagnant experiments was the cold air temperature cooling the surface water, which together with brine release made the surface water dense and induced convection. During melting periods the air temperature was stabilising and the water in the tank was quiescent. From the four investigated stagnant experiments, only experiment 32 with freezing and increased F_b, fulfilled the requirement of k proportional to $k^{-2/3}$ during a short wavenumber range. In the TKE equation buoyancy production was expected to dominate together with dissipation during stagnant experiments, and shear production could be assumed negligible. Due to the lack of sustained turbulence (see Figure 4.9b), no characteristic λ could be found to calculate ϵ and P_S, and hence no comparison of the terms in equation 2.2.7 was made for the stagnant experiments.

The results from this section will be discussed in Section 5.2.

4.3 Heat and salt flux estimates

In this section the results from the four different techniques to estimate heat and salt fluxes are presented for various experiments. At the end of the section there is a summary to compare the different methods, and give an overview of the mean heat and salt fluxes.

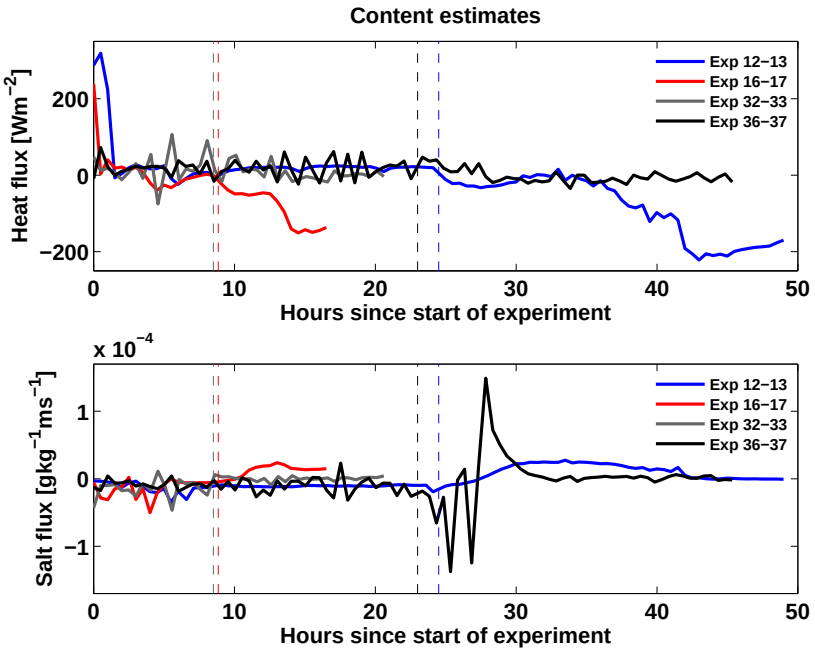

Figure 4.11: Heat and salt fluxes, presented as half an hour means, calculated from content method during all experiments. Top panel shows heat flux and lower panel salt flux. The dashed vertical lines indicate change from freezing to melting experiment.

4.3.1 Heat and salt content estimates

The content heat flux was strongly positive during the first few hours of current freezing experiments due to the strong decay in temperature (Figure 4.11). As the ice consolidated the heat flux fluctuated around zero, with values of ± 40 Wm^{-2}. After onset of melting the content heat flux was negative during current experiments, first weakly before it was strongly negative after the ice had disappeared reaching values down to -260 Wm^{-2} during experiment 13. During stagnant experiments the content heat flux was varying with values between 80 Wm^{-2} and -20 Wm^{-2}.

The content salt estimates were mainly negative during current freezing experiments, and the first few hours of melting experiments, before they turned positive for the latter part. During stagnant experiments the content salt flux did not show the same change in sign from freezing to melting, but rather fluctuated around zero.

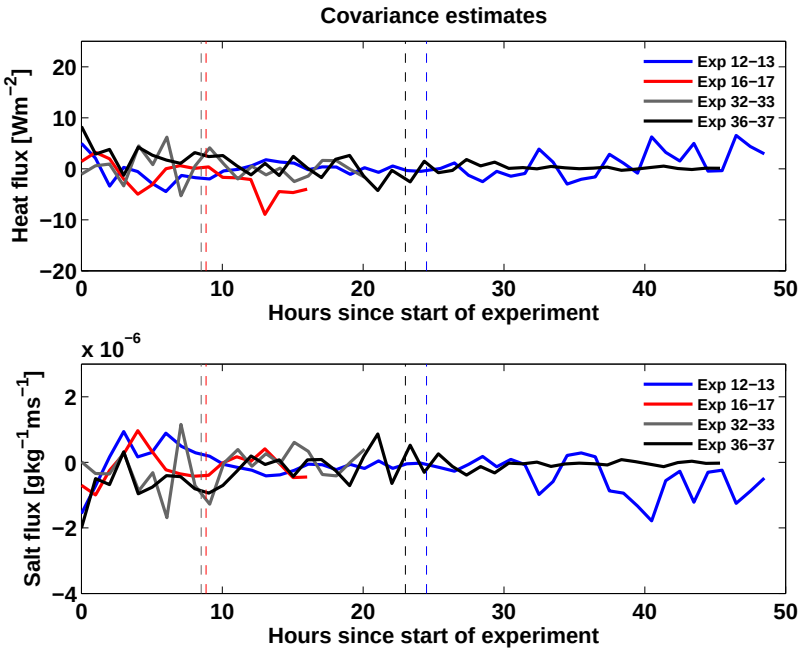

Figure 4.12: Heat and salt fluxes, presented as hour means, calculated from covariance method during all experiments. Top panel shows heat flux and lower panel salt flux. The dashed vertical lines indicate change from freezing to melting experiment.

4.3.2 Covariance estimates

The covariance estimate of heat flux was small during all experiments compared to the content method. It was varying between $\pm$ 10 Wm^{-2} (Figure 4.12), comparable to the content estimates during the periods of ice cover. The covariance salt flux was one order of magnitude lower than the content salt flux for all experiments, and varying between positive and negative values. It was not possible to detect any typical sign from the covariance method.

4.3.3 Residual method

The approximation to ice thickness presented in Figure 4.4a and 4.4c might be valid at the thermistorstring, but due to the inhomogeneous ice thickness during current experiments it could not be assumed representative for the whole tank. Due to a need for ice thickness measurements the residual method was only applicable for the stagnant freezing experiments. The method was used for both measured ice thickness and ice thickness approximated by a power fit to the measurements on the form $h = ax^b + c$.

The measured and fitted ice thickness were both interpolated to a temporal resolution of 10 minutes and a vertical resolution corresponding to that of the thermistor string. To calculate F_C from equation 3.2.5a, T_f was calculated with the top CTD salinity through equation A.3.1. T_0 was chosen as the sensor on the thermistorstring assumed to be at the surface.

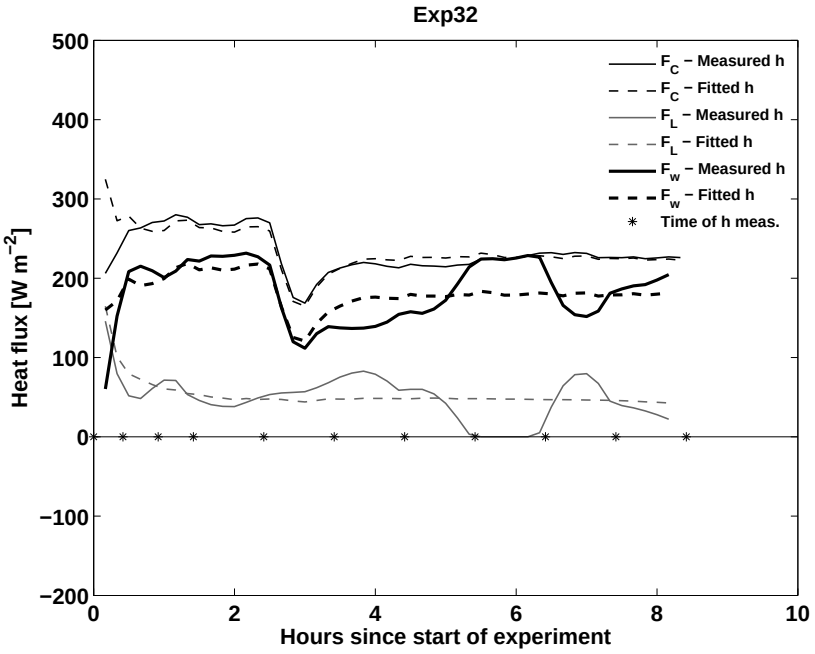

Figure 4.13: Oceanic heat flux estimated from residual method during stagnant experiment 32.

Figure 4.13 shows the different fluxes from the residual method during experiment 32. F_C was strongest in the beginning of the experiment, before it stabilised around 220 Wm^{-2} after four hours, and showed similar values for both inferred and measured ice thickness. F_L was strongest in the beginning with values up to 160 Wm^{-2} due to a fast ice growth, following from equation 3.2.5b, and decreased towards the end of the experiment ending up with values close to 50 Wm^{-2}. As a result F_w was smallest the first hours of the experiment when F_L was largest. F_w grew towards the end of the experiment as the latent heat release decreased, but the conduction through the ice remained the same.

4.3.4 Spectral method

The spectral method was dependent on turbulent water, and was hence only applied to the current experiments. During the stagnant experiments a convective system was

governing the water during freezing, and a stable calm stratification during melting and no well developed turbulence was sustained in the tank.

This technique does not take into account the sign of the flux, and only the magnitude was plotted in Figure 4.14. To apply this method the time series of w', T' and S' was needed, and through the procedure presented in Section 3.2.4 and equations 3.2.10 and 3.2.11, the heat and salt fluxes could be calculated. The heat flux was strong during the first hours when there still was open water in the tank and an efficient heat exchange between water and air. After the surface was consolidated, the absolute value of the heat flux remained close to 30 Wm^{-2}. After onset of melting the heat flux magnitude again increased towards 80 Wm^{-2}. This was expected to be a negative flux due to the water gaining heat from the air.

The salt flux showed a similar pattern as the heat flux, with strong heat flux corresponding to strong salt flux. During experiment 12 the flux was expected to be negative, and during experiment 13 positive (cf Figure 2.3).

4.3.5 Summary

All the mean values of turbulent surface heat and salt fluxes are compared in Table 4.2. In current freezing experiments the mean values of the fluxes were calculated from the time the water temperature was below -1.6 °C. The mean values during current melting experiments were calculated in the mirrored time interval of the freezing experiments. During stagnant experiments, the mean fluxes were calculated for the time interval the freezing experiments lasted, during both freezing and melting experiments. The covariance method showed the lowest values, and all values were close to zero for the heat flux. The covariance salt flux were two orders of magnitude smaller than when the other methods where used. The content method gave larger estimates, and during current experiments the sign followed what was expected for both heat and salt fluxes (cf Figure 2.3), except the heat flux during experiment 16. During the stagnant experiments both salt and heat fluxes from the content method were negative, except for the heat flux during experiment 36. The residual method showed higher heat flux estimates than the other methods, with a positive sign for the two experiments it was calculated for. The spectral method had magnitudes close to the content flux, but no sign could be evaluated since it was only given in absolute values. The calculations of the mean values for the spectral estimate might be comparably larger than the other estimates since the mean value was calculated for only positive values.

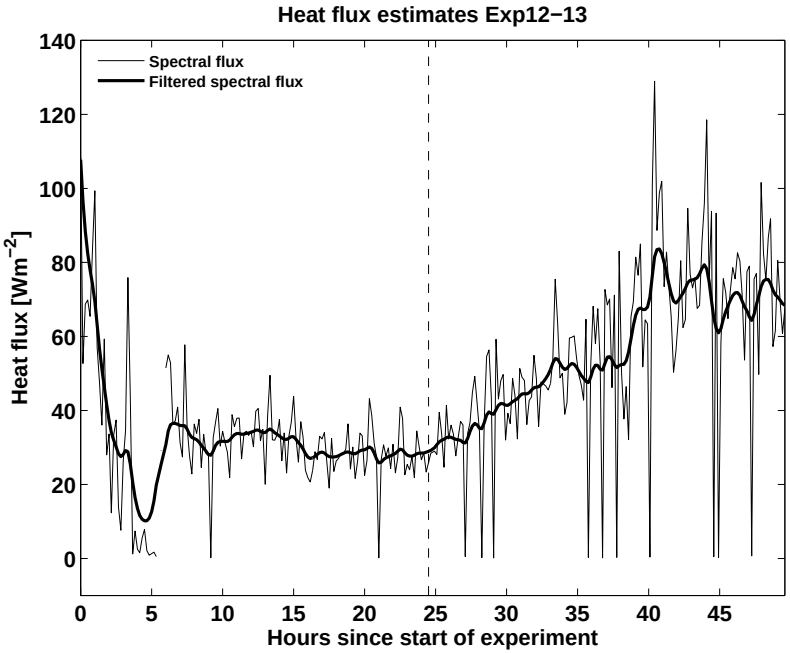

(a)

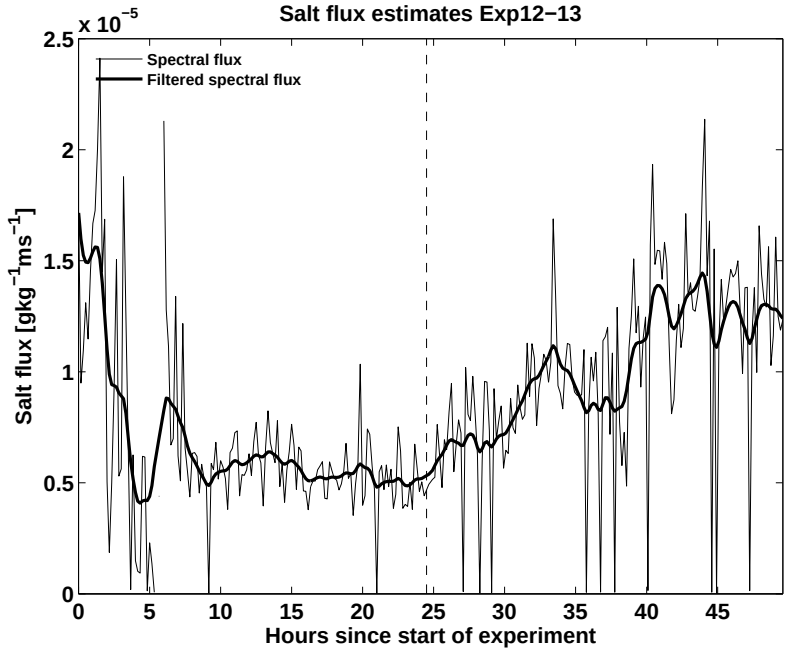

(b)

Figure 4.14: (a) Heat flux and (b) salt flux estimates in absolute values by the spectral method. The thin line is the flux in ten minute intervals, and the thick line is a low-pass filtered flux. Dashed vertical line indicates change from experiment 12 to 13.

The different methods and flux estimates will be discussed in Section 5.3.

	Covariance		Content		Residual	Spectral	
Exp	$\overline{F_w}$	$\overline{F_S}$ (10^{-7})	$\overline{F_w}$	$\overline{F_S}$ (10^{-5})	$\overline{F_w}$	$\overline{\lvert F_w \rvert}$	$\overline{\lvert F_S \rvert}$ (10^{-5})
12	-0.43	-1.91	19.43	-1.21	-	30.03	0.63
13	0.93	4.64	-78.89	1.08	-	54.11	0.98
16	-0.15	-4.89	2.49	-1.41	-	27.37	0.70
17	-3.14	-1.27	-85.40	1.16	-	64.38	1.13
32	0.39	-2.71	-18.43	-1.45	102.76	-	-
33	1.08	-0.93	13.33	-1.00	-	-	-
36	1.31	-3.80	18.17	-0.98	20.80	-	-
37	0.14	-1.19	-2.74	0.06	-	-	-

Table 4.2: Mean values of heat fluxes [Wm^{-2}] and salt fluxes [gkg^{-1} m s^{-1}] by the different methods.

4.4 Brine plumes

This section will present the results considering the brine plumes, and give some examples of the strength of the fluxes during plume events and their contribution to the heat and salt balances in the tank. During freezing experiments with a room temperature of -15 °C, the ice surface typically had a temperature of around -7 °C, measured by the thermistor string. Brine salinity is fixed for a given temperature [Notz, 2005] and when the brine left the ice it had a greater salinity than the underlying water, and a lower temperature. This also occurred during melting conditions when the brine still was colder than the underlying water, and hence had a higher salinity. Brine plumes were detected during all experiments and aligned and averaged as described in Section 3.3.

In Table 4.3 the brine plume characteristics for all experiments are presented. The current experiments showed stronger maximum F_w and minimum F_S values during plumes than the stagnant experiments. The typical duration time for a plume was longer during stagnant experiments than during current experiments, leading to comparable size for the mean values of the fluxes during plumes.

As an example of plume characteristics, Figures 4.15 and 4.16 show results from experiments 12 and 17 during freezing and melting respectively. Figure 4.15 shows the mean structure of w', S' and T' for experiment 12 and experiment 17 during brine plumes,

Exp	n	F_{wmax}	F_{Smin}	$\overline{F_{wplume}}$	$\overline{F_{Splume}}$	t
12	47	189.11	-6.60 $\cdot 10^{-5}$	80.65	-2.46 $\cdot 10^{-5}$	4.1
13	58	182.52	-6.73 $\cdot 10^{-5}$	73.16	-2.69 $\cdot 10^{-5}$	3.6
16	3	77.76	-17.72 $\cdot 10^{-5}$	-7.12	-0.54 $\cdot 10^{-5}$	3.6
17	23	320.88	-9.14 $\cdot 10^{-5}$	111.21	-3.79 $\cdot 10^{-5}$	3.4
32	66	92.31	-2.39 $\cdot 10^{-5}$	54.25	-1.40 $\cdot 10^{-5}$	7.1
33	73	60.60	-1.58 $\cdot 10^{-5}$	38.76	-1.01 $\cdot 10^{-5}$	5.0
36	120	111.50	-2.82 $\cdot 10^{-5}$	66.45	-1.70 $\cdot 10^{-5}$	4.7
37	109	48.23	-1.25 $\cdot 10^{-5}$	28.92	-0.74 $\cdot 10^{-5}$	5.1

Table 4.3: Brine plume characteristics for all experiments. n is number of detected plumes, F_{wmax} [Wm^{-2}] is maximum heat flux of the mean plume signal, F_{Smin} [gkg^{-1}m s^{-1}] is the minimum salt flux of the mean plume signal, $\overline{F_{wplume}}$ [Wm^{-2}] and $\overline{F_{Splume}}$ [gkg^{-1}m s^{-1}] are the mean heat and salt flux respectively during the mean duration time of the mean plume signal, and [s] is the mean duration time of detected plumes.

with the 95% confidence interval indicated by grey shading. 25 seconds on each side of the maximum value of the fluxes were plotted to represent the typical structure. A typical duration for a brine plume was 4.5 seconds and in Figure 4.16 the heat and salt fluxes were plotted to represent the typical structure. During the plumes F_w was closely negatively correlated with the negative F_S. The positive heat flux resulted from cold brine ($T' < 0$) sinking down ($w' < 0$). The maximum value exceeded 200 Wm^{-2} as an instantaneous flux during experiment 12, and 300 Wm^{-2} during experiment 17. This was clearly higher than the mean covariance values of -0.43 Wm^{-2} and -3.14 Wm^{-2} during experiment 12 and experiment 17 respectively (see Table 4.2). These results will be further discussed in Section 5.4.

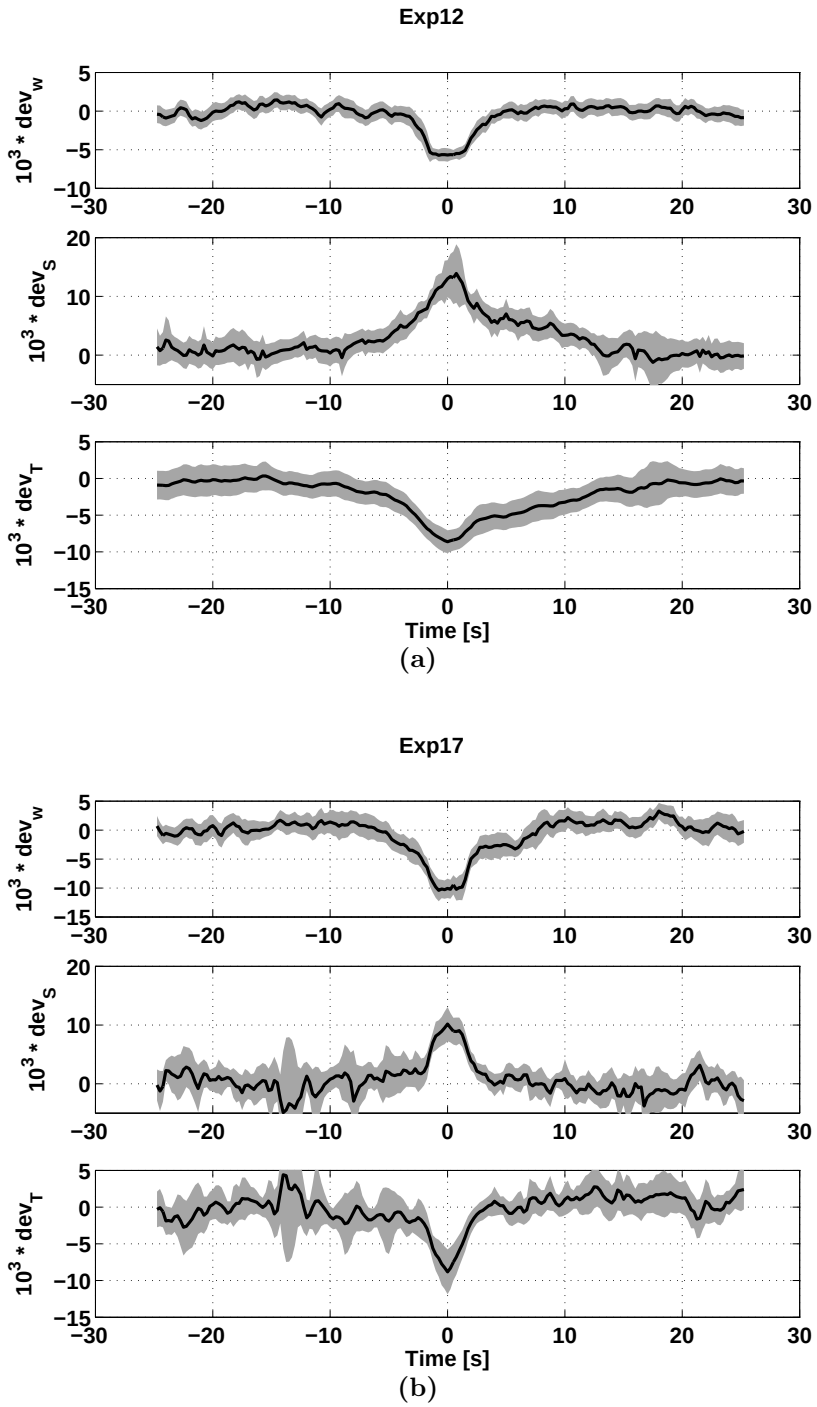

Figure 4.15: Mean structure of w', S' and T' for (a) experiment 12 and (b) experiment 17 during plumes. Grey shading indicates 95% confidence interval. Time is centred around the middle of the mean $\langle w'S' \rangle$ plume signal.

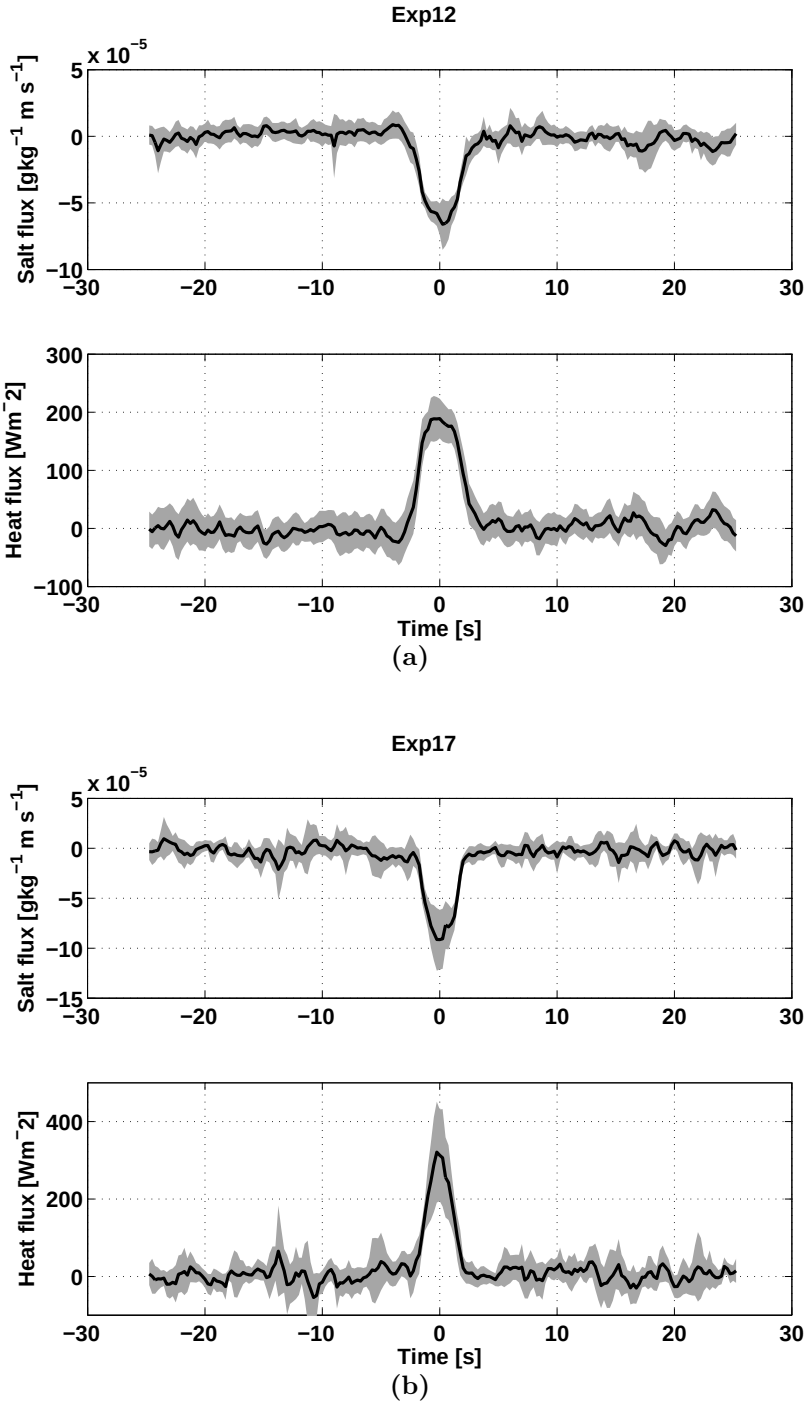

Figure 4.16: Mean fluxes in brine plumes during (a) experiment 12 and (b) experiment 17. In both (a) and (b) the top panel shows mean salt flux and bottom panel mean heat flux during all plume events. Grey shading indicated 95% confidence interval. Time is centred around the middle of the mean $\langle w'S' \rangle$ plume signal.

5

Discussion

This chapter contains a discussion of the main results from the experiments. There will first be an overall description of the temperature and salinity development and the resulting differences from experiment to experiment in Section 5.1. Thereafter the focus will be on the different terms in the TKE equation in Section 5.2, before moving on to discussing the flux estimates in Section 5.3. In Section 5.4 the brine plumes and their importance will be discussed. In the last section (5.5), the different uncertainties and errors will be evaluated.

5.1 Heat and salt budgets

Freezing experiments

In general the vertically averaged temperature was close to constant or increasing during all freezing experiments. This was a result of the reduced F_w after ice had collected at the surface (Figure 4.11), and the release of latent heat during this ice formation. The minimum temperature was different for current and stagnant experiments, where the current experiments reached 0.15 °C - 0.25 °C lower values than the stagnant experiments. This was due to the strong mixing from the wind and current during current experiments, leading to a cooling of the whole water column to T_f before onset of freezing, whereas during stagnant experiments only the top centimetres was cooled to T_f before freezing started. The lower minimum temperature during experiment 16

compared to experiment 12 resulted from a higher initial salinity depressing the freezing point. The increase in temperature during stagnant experiment 32 was larger than during experiment 36 due to the enhanced bottom heat flux during experiment 32, increasing the heat content of the tank. Since the water did not reach temperatures close to the bulk freezing point during the stagnant experiments, there must be a strong stratification in the top centimetres of the water column due to the ice forming at the surface.

Experiment 16 had increased wind speed compared to experiment 12, which lead to a faster ice growth and stronger salination of the water during the first eight hours with 0.06 g/kg h^{-1} in experiment 16 compared to 0.05 g/kg h^{-1} in experiment 12. The increase in salinity during current freezing experiments was fastest the first 6-7 hours, before it slowed down. This was due to the fast ice growth of thin ice and the following desalination of the ice. Naumann [2011] found that the bulk salinity of the ice grown in the current experiments decreased with 2.24 g/kg h^{-1} the first seven hours, before the desalination of the ice slowed down to 0.02 g/kg h^{-1} after seven hours. The salinity increased linearly with 0.06 g/kg h^{-1} the first eight hours of experiment 32, about twice as much as for the same time period during experiment 36 where it increased 0.03 g/kg h^{-1}. This was contradictory to what was expected from a larger heat content in the tank expected to lead to slower ice formation.

When comparing the measured to the inferred ice thickness in experiment 36 (Figure 4.7c), T_f was deeper than the actual ice thickness. This implied that the ice thickness inferred from T_f was not representative for the actual ice thickness. The salinity measured at 8 cm depth might not represent the actual salinity at the interface, and even if it did not correspond well during quiet experiments, the water was well mixed during current experiments and this approximation might be better. It was the only approach for ice thickness during current experiments, and was hence included as a possible approximation.

Melting experiments

As the melting experiments started the mean temperature in the water increased. Experiment 13 had a slower increase of 0.03 °C h^{-1} the first eight hours, compared to an increase of 0.09 °C h^{-1} during the first eight hours of experiment 17. The difference between the experiments was the strong wind during experiment 17, which increased the energy exchange between water and air and lead to a more efficient warming of

the water. During the stagnant experiments the temperature decreased or remained constant the first five hours after onset of melting. No wind could distribute the warm air in the tank and no current could mix the water. After the temperatures started increasing steadily during experiment 33 and 37, the heating rate was 0.034 °C h^{-1} and 0.028 °C h^{-1} respectively, where the difference most likely results from the enhanced bottom heat flux during experiment 33.

The salinity increased for certain periods during all melting experiments. For the current experiments, the maximum salinity occurred after three and two hours during experiment 13 and 16 respectively. The increase from onset of melting experiment and until the peak value was reached, was 0.09 g/kg during experiment 13 and 0.02 g/kg during experiment 17. The difference was a result of the ice growing for a longer time and reaching a larger ice thickness in experiment 12 than in experiment 16, and hence contained more brine that could drain out. After the peak value was reached the salinity decreased steadily, due to dissolution of the ice. During experiment 33 the salinity remained constant at the same value as at the end of experiment 32. In experiment 37 there was a strong increase in salinity the first seven hours, before it stabilised at the same level as the end of experiment 36. This increase in salinity during melting will be discussed further in Section 5.4.

5.2 TKE

The terms in the TKE budget were calculated by the covariance estimates for fluxes and friction velocity. As will be discussed in Section 5.3 these fluxes were small compared to the other flux estimates. Following from this the absolute values of the terms in the TKE equation might be small compared to the actual values present, but were useful as a comparison of orders of magnitudes. Table 4.1 showed the mean values of the estimates of the terms during the current experiments. P_S was always positive, as expected, and contributes to the TKE. It was roughly half the size of ϵ. To sustain the turbulence in the tank, this indicated that the shear production originated at an other location than the site of the TIC instrumentation, and decreased along its path. Since the forcing of the current was on the CTD side of the tank (Figure 3.2a), it is reasonable that the TKE balance was negative at the TIC site and turbulence was decaying due to lack of turbulent forcing. McPhee [1994] point out that in shallow measurements the requirement of horizontal homogeneity in the simplification of the TKE equation might not be fulfilled, leading to a difference in the TKE production

and dissipation. If the turbulence in the tank was not uniform, as suggested by the P_S and ϵ values, it supports the idea that advection of heat with the current lead to different flux estimates using covariance and content method.

P_B in Table 4.1 was two orders of magnitude smaller than the other terms. It was changing sign from freezing to melting experiments, being positive during freezing due to a cooling and salt release at the surface giving an unstable density gradient and hence increasing the TKE in the tank. During melting P_B was negative and stabilising the water, acting as a sink of TKE. The total contribution during current experiments however were negligible.

Mean values of λ during the experiments varied between 0.02 m and 0.04 m at ADV1 site and 0.05 m and 0.06 m at ADV2 site. The decreased mixing length downstream corresponds to the dissipation of turbulence and a decay in turbulent forcing. The mixing lengths found were relatively small compared to values found by McPhee [2008b]. He found his lowest values closest to the interface and had values of λ down to 0.3 m, 2 m from the boundary. In the surface layer, extending from the ice water interface and downwards, mixing length increases approximately linearly with depth following the simple relationship $\lambda = k|z|$ [McPhee and Morison, 2001], where k = 0.4 is von Kàrmàns constant. This is valid in neutral conditions when buoyancy forcing is negligible compared to shear production, which was valid during the current experiments. When using this relationship for the TIC depth of 0.2 m it results in $\lambda = 0.08$ m. This was larger than the estimates from the experiments, but still in the same order of magnitude.

When looking at the time development of λ it was larger during the beginning of freezing experiment 16. Experiment 12 did not show corresponding high values. During experiment 16 the wind speed was increased compared to the other experiments, and the water was kept open for a longer period than during experiments with lower wind speed. It takes approximately four hours before λ decreases remarkably during experiment 16. When comparing this to pictures of the ice cover, the TIC side was closed at that time, but remained open on the CTD side.

During the stagnant experiments, only experiment 32 showed a developed turbulence spectrum over a short range of wavenumbers. This was the experiment with enhanced bottom heat flux of 31 Wm^{-2} and freezing at the surface. Experiment 36 with the same surface forcing did not show any developed turbulence, which indicated that an increased bottom heat flux could enhance the mixing in the water sufficiently to fulfil the requirement of a -2/3 gradient in the inertial subrange.

5.3 Methods for estimating fluxes

Four different methods were used to quantify the heat and salt fluxes in the tank. The most common way to calculate fluxes from turbulence measurements from the TIC is directly from the deviatory time series through the covariance method. This is a standard method, and turned out not necessarily being representative for the overall fluxes in the tank. When comparing the covariance fluxes to the content heat and salt fluxes they were considerably lower, sometimes as much as two orders of magnitudes.

In general when comparing the temperature and salinity development in the water during ice growth and melting with calculated fluxes, the fluxes were strongest while there was open water in the tank, with values close to those found by Sirevaag [2009] in the marginal ice zone. Annual average values of ocean heat flux in the Arctic are small, and Perovich and Elder [2002] found values of 7-8 Wm^{-2} under multiyear ice corresponding to the values in the tank after the ice cover was closed. It was not possible to distinguish the strength of the fluxes during the early periods of freezing from the later periods. During the stagnant experiments the ice cover closed after less than half an hour, and the fluxes were smaller than during current experiments.

The content method was the most direct, calculated from the vertically averaged temperature an salinity development in the tank, and the constant F_b. This represented the total heat and salt fluxes in the tank. F_b was held as a constant value during each experiment and will not be discussed further in this section. Due to the large differences in ice thickness and ice cover in the tank during current experiments, it was plausible that the cooling of the water took place on the more turbulent CTD-side of the tank, and was advected horizontally with the current to be measured by the TIC. This could possibly explain the smaller covariance heat flux estimate, compared to a larger value in the content estimate. As an example the content heat flux during experiment 12 was very large in the beginning when there was open water, but came closer to the covariance fluxes after the ice cover closed and the surface forcing was more equal throughout the tank. Following this argument the covariance estimates were thought of as valid for the site of the TIC, but weaker than, and not resolving the overall fluxes present in the tank.

The residual method was an approach to try to close the total heat budget in the tank under simple assumptions during stagnant freezing experiments. The conducted heat flux was relatively constant throughout experiment 32, and did not decrease as was expected due to thicker ice. Instead the expected decrease was equalised by the in-

creased temperature difference between the freezing point and the surface temperature as the ice grew thicker. The latent heat flux was large due to the fast ice growth of thin ice. Totally this lead to a residual oceanic heat flux that increased in the beginning of experiment 32, then stabilised at 180 Wm^{-2}. This did not correspond to the content heat flux, which showed mean values of 18 Wm^{-2} during experiment 32 and experiment 36. The applicability of this method was limited due to the need of measured ice thickness, and the results were sensitive to both ice thickness and which temperature-sensors were chosen to represent the gradient through the ice. When doing the manual ice thickness measurements with a ruler, it was not possible to read the thickness with a better resolution than close to every 2 mm. If the ice thickness was e.g. 2 mm larger than what was measured, the conducted heat flux would decrease with as much as 25 Wm^{-2}. If a sensor 5 mm higher on the thermistorstring was chosen to be the surface temperature, F_C would increase with 70 Wm^{-2}. This together with F_L being dependent on the ice growth rate, and hence indirectly dependent on the ice measurements, lead to large uncertainties using this method.

The heat and salt fluxes estimated by the spectral method gave higher values than the covariance method, and in the same order of magnitude as the content estimates. The fluxes were estimated using the same constants for $c_\gamma = 0.48$ and $c_T = 0.83$ as McPhee [2004]. By using experiment data, c_γ was estimated for the two sets of current experiments, 12-13 and 16-17, and the values turned out to be 1.82 and 2.09 respectively. This gave no visible changes in the calculation of the fluxes, and was not used in the figures presented. The expansion to a calculation of salt flux was straight forward under the assumption that c_T had a corresponding value for a constant c_S with the same numeric value. This would be valid when assuming that mixing of heat and salt were equally efficient, as is expected in a turbulent flow. The spectral method showed a similar shape as the content estimates, with a strong flux in the beginning, then decreasing, and as the room temperature was turned to melting it again increased. This seems reasonable when considering the general turbulence, and the waters ability to exchange heat due to the ice cover.

In this technique the buoyancy forces were assumed negligible, which McPhee [2004] claims valid under thick ice away from margins. The ice in the tank was thin and definitely affected by margins, but by considering table 4.1, P_B was two orders of magnitudes smaller than P_S and ϵ. The assumption might therefore be valid during the experiments, but for other reasons than suggested by McPhee [2004].

Summary heat and salt fluxes

The content method gave the most reliable estimates of the fluxes actual present in the tank. The covariance estimates underestimated the fluxes with as much as up to two orders of magnitudes, and were only representative at the TIC location. The residual method was sensitive to temperature and ice thickness, and seemed to overestimate the fluxes compared to the content method. The spectral method gave promising results, but unfortunately no sign could be evaluated.

5.4 Brine plumes

In the experiments brine plumes could be detected for cold air temperatures, of -15 °C implying freezing, where the brine drained out due to gravity. Interestingly the brine plumes also took place during melting conditions at the surface, when the room temperature was set to +5 °C, where one traditionally expected the salt flux to be positive because of release of melt water. An explanation to this was connected to the permeability of the ice. The permeability increased as the temperature increased, which lead to a decreased solid fraction due to an increased number of inter-connected brine pockets. As the ice got more permeable the brine pockets opened up, also at the interface between water and ice, and the diluted brine drained out. Another possible contribution to the brine plume release during melting, especially during current experiments, was surface meltponds leading to flushing and replacement of brine with fresher water from melted surface ice.

After the stagnant melting periods the ice had approximately the same thickness as at onset of melting, but the permeability was strongly increased and the ice was soft and fragile due to the low solid fraction. During one of the stagnant test experiments (autumn 2010) all the ice melted and there was a clear stratification in the top centimetres of the water which could be seen visually. The fresh melt water was lying on top of the saline water underneath, since brine had drained out before the pure ice started melting at 0 °C. The light meltwater was isolated from the underlying water and only mixed down through diffusion. This stable stratification was seen in the salinity data and supported the idea that the brine was lost before the fresh solid ice started melting.

The brine plumes were detected from the covariance fluxes. Since these probably were weaker than the actual fluxes, this signal was also weaker, but still visible. Figure 4.16a and 4.16b showed the salt and heat fluxes of plumes during experiment 12 and 17 with

95 % confidence interval. The confidence interval was largest at the center of the plume since the strength of each plume varied, and was by definition centred around zero.

Importance of fluxes during brine plume events

The importance of the brine plume fluxes were compared relative to the salt and heat fluxes from the content method to get the contribution to the total heat and salt budgets in the tank. Overall the importance of the fluxes were small, and often less than 3 %, see Table 5.1. This indicated that the large instantaneous fluxes had a too short duration to substantially effect the heat and salt budgets in the tank, and that the averaging period of 10 minutes evened out the large absolute values of the brine plume fluxes.

During current experiments the plume fluxes were enhancing the fluxes in the tank during freezing, and counteracting them during melting, as expected. The exception was the heat flux during experiment 16, but since this experiment only had three detected plume events this result was not emphasised. In the stagnant experiments the plume fluxes enhanced the fluxes in the tank except during experiment 37, where the salinity difference from the start to the end of the experiment was only 0.01 g/kg. The content salt estimate was hence lower than during the other experiments, and the brine plumes would therefore get an artificial high importance. In experiment 32 the water in the tank became warmer during freezing, which was contradictory to what was expected. This was a result of the increased bottom heat flux, which heated the water even if both brine plumes and F_w were cooling it. In experiment 33, F_w was cooling the surface, but the temperature increased due to the strong bottom heat flux. For salinity, the overall fluxes in the tank were negative both during melting and freezing, and the plume salt flux was enhancing the flux in the tank.

The correlation between the heat flux and the salt flux using 10-min fluxes were negative for all experiments. During the plume events the average correlation was $R_{plumes} \sim -0.98$ between the salt flux and the heat flux, and for the whole record of the 10-min means the average correlation was $R \sim -0.79$. The correlation coefficients between F_w and F_S for the 10-min means and the plumes are listed in table 5.1.

During the melting in experiment 37 the salinity strongly increased the first 2-7 hours in the top 20 cm (Figure 4.6d). At the same time the temperature showed a weak decrease (Figure 4.6c). When comparing this with the plume event distribution (Figure 5.1) it corresponded very well to the changes in salinity and temperature, where 108 of 109

Exp	% F_w	% F_S	R	R_{plumes}	n
12	2.0	1.0	-0.54	-0.98	47
13	-0.5	-1.3	-0.62	-0.98	39
16	-0.02	0.2	-0.31	0.39	3
17	-0.6	-1.5	-0.79	-0.97	23
32	6.3	2.0	-0.97	-0.99	66
33	4.1	1.4	-0.98	-0.99	73
36	3.0	1.4	-0.98	-0.99	120
37	-9.9	-11.9	-0.95	-0.99	109

Table 5.1: The percentage of the total flux during the time of the plumes. Negative sign means that the plume fluxes counteracted the overall fluxes. R and R_{plumes} were the correlation coefficients between F_w and F_S during the experiment and brine plume events respectively. n is the number of detected plumes during each experiment.

plume events in total were detected during the first seven hours. This strengthened the idea of brine plumes and that brine leaves the ice before the solid ice starts melting.

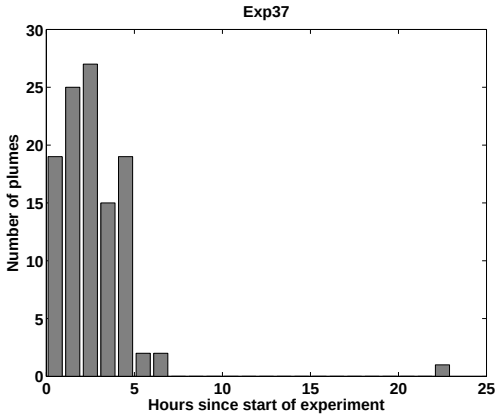

Figure 5.1: Plume event distribution during experiment 37.

Forcing of brine plumes - Rayleigh number

To decide the timing of onset of gravity drainage during current experiments the Rayleigh number for the middle of the ice was calculated. This was done for experiment 32 and 36 where ice thickness was measured, and are displayed in Figure 5.2 together with the plume distribution with time. Ra was calculated for each timestep where the ice thickness was measured and linearly interpolated between. The first few hours it increased rapidly before it started decreasing. The brine ejection should theoretically start after the Ra number has reached $Ra_c \sim 10$ [Notz and Worster, 2008]

when gravity drainage was possible, closely linked to the maximum Ra. The density difference between top and bottom of the ice, driving the brine plumes, would then be large enough to overcome the dissipative forces in diffusion and viscosity. Ra increased fast the first 1-2 hours and reached maximum values while the ice still was less than 1 cm. The observed plume distribution indicated a start of gravity drainage immediately after onset of freezing, see Figure 5.2a and 5.2b, close to the maximum Ra.

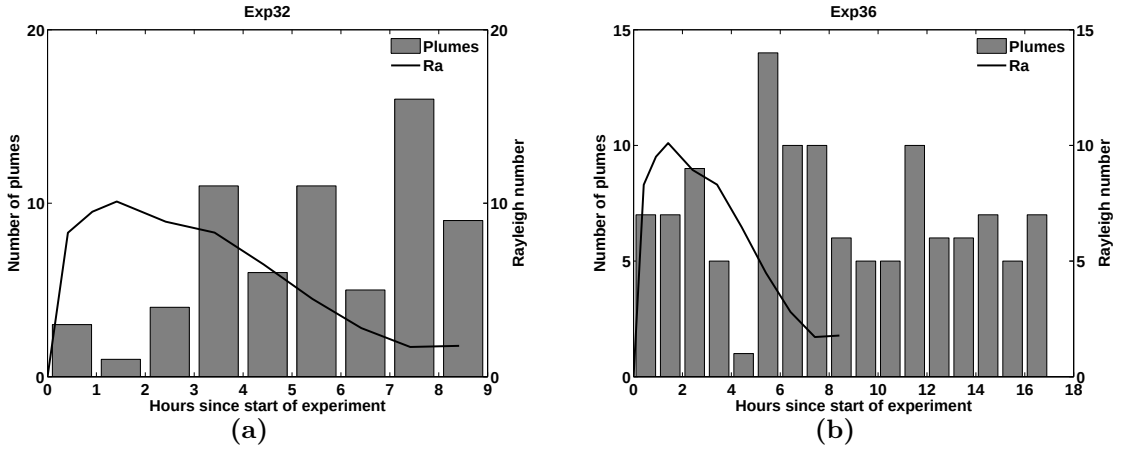

Figure 5.2: Rayleigh number and plume distribution during (a) experiment 32 and (b) experiment 36.

Comparison with Widell et al. [2006]

Widell et al. [2006] studied ejection of brine plumes under land-fast first-year sea ice from similar measurements as obtained in the tank. Their measurements were done under 1.2 m thick and even ice where the main current was tides. They observed that under conditions implying melting at the ice-ocean interface, there was a strong negative salt flux correlated with a positive heat flux. The measurements indicated that an increased turbulent heat flux from below could play an important role in the desalination of sea ice through release of brine plumes.

When comparing the brine plume data obtained in the tank with Widell et al. [2006], the deviatory time series of temperature and salt were generally of equal magnitude. The deviatory vertical velocity however was smaller in the tank. This might be due to the fact that brine draining from thick ice could be accelerated to greater velocities before it left the ice base and started mixing with the underlying water. The total signal of $|\langle w'S'\rangle|$ would then be stronger for thicker ice. The movement in the tank was highly irregular over short timescales during current experiments, and the vertical

movement was affected by the surface forcing from both buoyancy and wind, and also the current. Following from this, the background turbulence in the tank was assumed large compared to the deviatory time series in the tank, and the conditions for the plume events having to be larger than 5 times the rms value was reduced to larger than the rms value. The resulting heat and salt fluxes during brine plumes in the tank were of comparable size as the measurements obtained by Widell et al. [2006]. The measurements in the tank and in Widell et al. [2006] were made in a different vertical distance from the ice base, 20 cm and 1 m respectively.

5.5 Uncertainties and errors

To do experiments in a tank gives an opportunity to study several realisations of the same situation under the same boundary conditions, leading to more than one dataset to compare. There were many uncertainties connected to doing experiments in a laboratory, both artificially introduced by being in a laboratory and the ones related to instrumentation. At the same time as it was possible to control the different parameters affecting the water, it was not given what would be the effect of them.

During the current experiments there were large differences in ice thickness, ice cover and turbulent forcing over the small surface area. The surface was very inhomogeneous and at the same time as there was open water in front of the air hose, the grease ice layer could be up to 20 cm thick in the short ends. The TIC was placed on one side of the division wall, and the CTDs on the other. Due to the non-symmetric current, being forced only at one point on the CTD side, the ice cover closed on the side where the TIC was placed up to five hours before it closed on the CTD side. This lead to a longer periods of cooling on the CTD side together with more turbulence created for a longer time. The CTDs were attached directly to the side wall and were possibly more directly influenced by the room temperature and the side wall heating than the TIC, which was placed in the middle of the tank. The side wall heating was not quantified and the direct effect of it was uncertain.

The shear from the current was not uniform throughout the tank. The water was moving fastest in the center of the tank, and slower towards the sides and the middle division wall due to friction. This means that the water spent more time close to the walls where the CTDs were placed, compared to the area of the TIC. The bottom heat flux introduced affected the heat content of the water, and especially the CTD at 85

cm depth during quiet experiments. This heat flux came from heating wires and was not covering the bottom, rather placed in a grid like pattern. The initial salinity was not the same for all experiments due to evaporation and ice sampling, which affected e.g. the freezing point of the water. This all together lead to large variations over small distances in the tank, and it was hard to say what exactly was the cause and what was the effect of each parameter.

6

Summary and outlook

Summary

In this work, results obtained from a series of lab experiments focusing on turbulence in the under ice boundary layer during growth of young sea ice are discussed. The experiments were conducted in a tank, where two different main setups, turbulent and stagnant water, were compared in terms of turbulence in the under ice boundary layer. High frequency measurements of temperature, conductivity and velocity were obtained and used to examine turbulent fluxes and the balance of the terms in the turbulent kinetic energy budget. The vertically averaged temperature in the tank during stagnant experiments was up to 0.25 °C higher than the bulk freezing point. This lead to the conclusion, since ice still was freezing at the surface, that there must be a strong temperature stratification in the top centimetres.

Four different estimation techniques for heat and salt fluxes have been compared. It turned out that the covariance method, which is the most common, did not resolve the actual fluxes present in the tank. This lead to three other methods for flux estimation, to try to quantify the fluxes. The heat and salt content method was direct and corresponded to the mean changes in salinity and temperature in the tank. The residual method had several drawbacks, and turned out not to be very reliable. The spectral method showed a satisfactory shape, but could not say anything about the sign of the flux. The content fluxes showed largest values the time when the water was open, as did also the spectral fluxes. During stagnant experiments the content fluxes were smaller than during current experiments due to the ice cover and the reduced

turbulence. Overall the content estimates were the most reliable, and together with the promising results from the spectral method these two estimates were trusted as representative for the fluxes in the tank.

In the evaluation of the TKE balance, dissipation and shear production were the main contributors. The turbulence was produced in front of the pump forcing the current, and dissipated further downstream. Following from this the turbulence in the tank was inhomogeneous with the main shear production and the main dissipation taking place at different sites. This lead to the conclusion that even though the covariance estimates were significantly lower than the content estimates, they were valid for the TIC site.

Brine plumes occurred both during freezing and melting experiments, leading to a desalination of the ice and a subsequent salination of the water underneath. This indicates that the ice releases its brine before the solid ice matrix starts to melt during a warming of the ice, due to an increased permeability and opening up of brine channels. The instantaneous values of the brine plume fluxes were large and up to two orders of magnitude larger than the mean values, but the total importance in the heat and salt balance was only ~ 3 %.

Outlook

After doing experiments one could always come up with other ideas of how to accomplish them, and new questions were raised throughout the experiments and data implementation period, to what was discovered. During quiet freezing experiments the temperature in the water was rising, but still the ice thickness increased. This indicates a strong stratification over a short vertical distance in the near surface water, and it could be interesting to investigate this more thoroughly. The wind introduced was not quantified and varied throughout the tank. No current experiments were accomplished without wind for comparison, and the actual effect of it still remains unknown.

To visualise the brine plumes leaving the ice it could be useful to do experiments where dye was added in the ice to see how brine drains at the ice base, and if it looks similar to e.g thermals leaving a heated surface (cf Section 2.2.4). Ideally longer experiments could have been conducted, to grow thicker ice and reduce the influence from the surface. Even if a lot of different parameters indeed were needed to get the setup as close to reality as possible, it could be useful the exclude some of them to get more control of the different parameters.

A

Appendix

A.1 Calibration of μC

The μC SBE7 sensor had a voltage drift in absolute value and it required calibration to find the absolute salinity. To solve this issue the SBE7 was calibrated against the accurate conductivity from the standard C sensor SBE4. Within 10 minute intervals a low-pass filter of 30 seconds was used to remove the short-term fluctuations and keep the longer trend of the signal. Any change on timescales longer than 30 seconds were assumed to be registered by the SBE4, whereas the SBE7 had a faster response time. Calibration coefficients together with error estimates were obtained from a linear fit of the accurate conductivity from SBE4 against the frequency signal of SBE7. The new calibration coefficients were applied to the raw data from SBE7 to calculate a new μC.

A.2 Temperature dependence of salinity

The salt used in the experiments was NaCl, the main salt constituent of seawater. The salinity was calculated from temperature and conductivity measurements, where the conductivity was temperature dependent. When temperature increases the conductivity will also increase, and further an increase in conductivity indicates increased salinity, even if no more salt is added to the water. When calculating salinity this dependency was compensated for by using the same equation as used for seawater.

As an example figure A.1 shows temperature, salinity and conductivity evolution from experiment 15. After all the ice was melted a further heating of the room lead to a temperature increase of the water, which in turn lead to an increase in conductivity. The salinity of the last part of experiment 15 stayed relatively constant during this temperature increase (Figure A.1), and this validated the equation used in the conversion from conductivity and temperature measurements to salinity. The absolute value of the salinity was however not directly corresponding to that of sea water. From accurate experiments, where the salinity was measured with a handhold multimeter for NaCl solutions and compared to results from the CTDs, the absolute value of NaCl salinity was between 0.6 - 1.0 g/kg lower than that for seawater [Naumann, 2011]. This correction was not taken into account during this thesis.

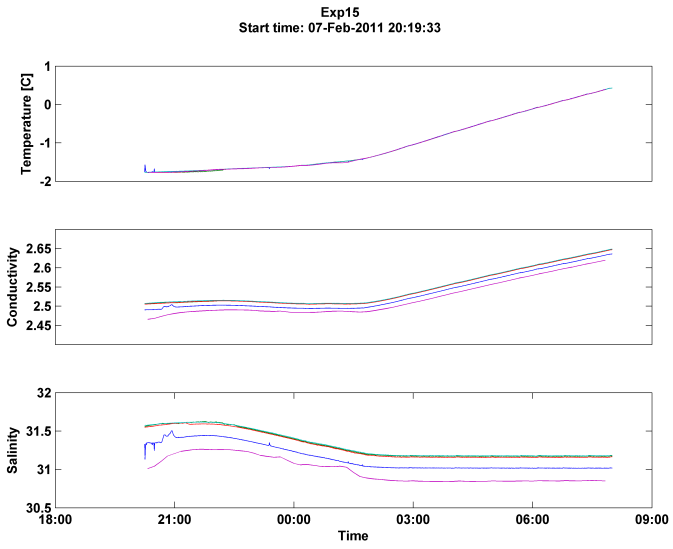

Figure A.1: Example of temperature, conductivity and salinity development during experiment 15.

A.3 Properties of sea ice

Weast [1971] gives data for the freezing point of NaCl solutions which can be approximated by a polynomial

$$T_f = -0.0592S - 9.37 \cdot 10^{-6}S^2 - 5.33 \cdot 10^{-7}S^3, \tag{A.3.1}$$

valid for NaCl solutions with salinity between 1 and 230 g/kg.

The density for both brine and salt water can be obtained from data given in Weast [1971] valid for NaCl solutions at 20 °C,

$$\rho_{20} = 998.43 + 0.69722S + 2.5201 \cdot 10^{-4}S^2, \tag{A.3.2}$$

where S is the salinity between 1 and 260 g/kg. The maximum error from using this equation at lower temperatures is less than 2% down to a temperature of -20 °C [Notz, 2005].

When sea water freezes or melts, the phase change requires a release or absorption of heat. This latent heat of fusion can be described by the polynomial fit [Notz, 2005]

$$L = 333700 + 762.7T + 7.929T^2. \tag{A.3.3}$$

For $T = -1.8°C$ $L = 332300 Jkg^{-1}$, which is used in this work.

B

Appendix

B.1 Overview of experiments

Table B.1: Overview of experiments

EXP	Date Time	Filename	T_a	Motion	Comment
	31.01	31.68	-1°C	Current	
	01.02	32.39 32.56	-20°C	Current	
EXP 10	02.02 09:15 02.02 16:20	33.38	-10°C	Wind and current	
EXP 11	02.02 16:20 03.02 08:00	33.68	0°C	Wind and current	
	03.02	34.67	-20°C	Wind and current	
EXP 12	04.02 09:45 05.02 10:08	35.40 35.67	-15°C	Wind and current	
EXP 13	05.02 10:08 06.02 11:25	36.43	+5°C	Wind and current	
	06.02.11	37.49	-2°C	Wind and current	
EXP 14	07.02 15:36 07.02 20:15	38.65	-15°C	Wind and current	
EXP 15	07.02 20:15 08.02 08:00	38.84	5°C	Wind and current	
EXP 16	08.02 13:45 08.02 22:34	39.57	-15°C	Wind and current	
EXP 17	08.02 22:34 09.02 07:25	39.94	5°C	Wind and current	
EXP 18	09.02 10:45 10.02 10:20	40.44 40.51 40.67	-5°C	Wind and current	

Continued on next page

Table B.1 – continued from previous page

EXP	Date Time	Filename	T_a	Motion	Comment
		40.85			not complete file
	10.02	41.35			
		41.35a			
EXP 19	10.02 10:20	41.41	+5°C	Wind and current	not complete melting
	10.02 12:00				
EXP 20	10.02 15:05	41.63	-20°C	Wind and current	
	10.02 21:00	41.73			
EXP 21	10.02 21:00	41.87	+5°C	Wind and current	
	11.02 06:50				
	11.02	41.41	-10°C	Wind and current	
EXP 22	11.02 10:00	42.42	-10°C	Wind and current	
	12.02 20:00	42.47			ADV not logging
		42.47a			
		42.63			ADV not logging
		42.64a			
					Instruments frozen
		43.37	-10°C		
EXP 23	12.02 20:00	43.83	+5°C	Wind and current	
	13.02 12:30				
(EXP 24)	13.02	44.53	-2°C	Current	
(EXP 25)	14.02	45.73	-20°C	Current	
EXP 30	16.02 08:30	47.35	-10°C	No motion	
	16.02 17:55	47.62			
EXP 31	16.02 17:55	47.75	+5°C	No motion	
	17.02 07:35				
EXP 32	17.02 09:35	48.40	-15°	No motion	$F_w = 31[Wm^{-2}]$
	17.02 18:00	48.56			
EXP 33	17.02 18:00	48.75	+5°C	No motion	$F_w = 31[Wm^{-2}]$
	18.02 07:22				
EXP 34	18.02 09:00	49.37	-20°C	No motion	
	18.02 17:00	49.59			
EXP 35	18.02	49.72	+5°C	No motion	
	19.02 08:50				
EXP 36	19.02 09:45	50.40	-15°C	No motion	
	20.02 08:50	50.40a			
		50.55			
		50.66			
EXP 37	20.02 08:50	51.38	+5°C	No motion	
	21.02 08:10				
(EXP 38)	22.02	53.56	-15°C	Standing wave 1	
EXP 40	22.02 10:40	53.45	-15°C	Standing wave 1	
	222.02 18:20	53.66			
EXP 41	22.02 18:20	53.76	+5°C	Standing wave 1 + fan	
	23.02 08:05				
EXP 42	23.02 11:10	54.47	-10°C	Standing wave 1	
	23.02 21:40	54.57	-20°C		
EXP 43	23.02 21:40	54.90	+5°C	Standing wave 1 + fan	
	24.02 08:20				

References

Aagaard, K., and Carmack, E. (1989). The role of sea ice and other fresh water in the Arctic circulation. *Journal of Geophysical Research*, *94*(C10), 14485–14498.

Aagaard, K., Coachman, L., and Carmack, E. (1981). On the halocline of the Arctic Ocean. *Deep Sea Research Part A. Oceanographic Research Papers*, *28*(6), 529–545.

Comiso, J. (2002). A rapidly declining perennial sea ice cover in the Arctic. *Geophysical Research Letters*, *29*(20), 1956.

Comiso, J. (2008). Large-scale Characteristics and Variability of the Global Sea Ice Cover. In *Sea ice: An introduction to its physics, chemistry, biology and geology* (pp. 112–142). Oxford, UK: Blackwell Science Ltd.

Comiso, J., Parkinson, C., Gersten, R., and Stock, L. (2008). Accelerated decline in the Arctic sea ice cover. *Geophysical Research Letters*, *35*(1), L01703.

De La Rosa, S., Maus, S., and Kern, S. (2011). Thermodynamic investigation of an evolving grease to pancake ice field. *Annals of Glaciology*, *52*(57), 206–214. (Part 2)

Dieckmann, G., and Hellmer, H. (2003). The importance of sea ice: an overview. In *Sea ice: An introduction to its physics, chemistry, biology and geology* (pp. 1–21). Oxford, UK: Wiley Online Library.

Eicken, H. (2003). From the Microscopic, to the Macroscopic, to the Regional Scale: Growth, Microstructure and Properties of Sea Ice. In *Sea ice: An introduction to its*

physics, chemistry, biology and geology (pp. 22–81). Oxford, UK: Blackwell Science Ltd.

Freitag, J. (1999). *Untersuchungen zur hydrologie des Arktischen meereises: Konsequenzen für den kleinskaligen Stofftransport(in german).* Bremerhaven: Alfred-Wegener-Institut für Polar- und Meeresforschung.

Kelley, D. (1990). Fluxes through diffusive staircases: A new formulation. *Journal of Geophysical Research*, *95*(C3), 3365–3371.

Kester, D., Duedall, I., Connors, D., and Pytkowicz, R. (1967). Preparation of artificial seawater. *Limnology and Oceanography*, *12*(1), 176–179.

Leppäranta, M. (1993). A review of analytical models of sea-ice growth. *Atmosphere-Ocean*, *31*(1), 123–138.

Martin, S., and Kaufmann, P. (1981). A field and laboratory study of wave damping by grease ice. *Journal of Glaciology*, *27*(96), 283–313.

Maykut, G. (1982). Large-scale heat exchange and ice production in the central Arctic. *Journal of Geophysical Research*, *87*(C10), 7971–7984.

McPhee, M. (1994). On the turbulent mixing length in the oceanic boundary layer. *Journal of physical oceanography*, *24*(9), 2014–2031.

McPhee, M. (2004). A spectral technique for estimating turbulent stress, scalar flux magnitude, and eddy viscosity in the ocean boundary layer under pack ice. *Journal of physical oceanography*, *34*(10), 2180–2188.

McPhee, M. (2008a). *Air-ice-ocean interaction: Turbulent ocean boundary layer exchange processes.* New York: Springer Science.

McPhee, M. (2008b). Physics of early summer ice/ocean exchanges in the western Weddell Sea during ISPOL. *Deep Sea Research Part II: Topical Studies in Oceanography*, *55*(8-9), 1075–1097.

McPhee, M., and Morison, J. (2001). Under-ice boundary layer. In *Encyclopedia of ocean sciences* (Vol. 6, pp. 3069–3076). San Diego, California: Academic.

McPhee, M., and Stanton, T. (1996). Turbulence in the statically unstable oceanic boundary layer under Arctic leads. *Journal of geophysical research*, *101*(C3), 6409–6428.

Morison, J., and Smith, J. (1981). Seasonal variations in the upper Arctic Ocean as observed at T-3. *Geophysical Research Letters*, *8*(7), 753–756.

Naumann, A. K. (2011). Physikalische Prozesse der Meereisentwicklung in offenem Wasser. *University of Hamburg*.

Notz, D. (2005). Thermodynamic and fluid-dynamical processes in sea ice. *University of Cambridge, Diss*.

Notz, D., and Worster, M. (2008). In situ measurements of the evolution of young sea ice. *Journal Geophysical Research*, *113*(C03001).

Notz, D., and Worster, M. (2009). Desalination processes of sea ice revisited. *Journal of Geophysical Research*, *114*.

Padman, L. (1995). Small-scale physical processes in the Arctic Ocean. In *Arctic Oceanography: Marginal Ice Zones and Continental Shelves* (pp. 97–129). Washington, DC: American Geophysical Union.

Perovich, D., and Elder, B. (2002). Estimates of ocean heat flux at SHEBA. *Geophysical research letters*, *29*(9), 1344.

Sirevaag, A. (2009). Turbulent exchange coefficients for the ice/ocean interface in case of rapid melting. *Geophysical Research Letters*, *36*(4), L04606.

Smedsrud, L. (2011). Grease-ice thickness parameterization. *Annals of Glaciology*, *52*(57), 77–82.

Steele, M., and Boyd, T. (1998). Retreat of the cold halocline layer in the Arctic Ocean. *Journal of Geophysical Research*, *103*(C5), 10419–10435.

Stroeve, J., Holland, M., Meier, W., Scambos, T., and Serreze, M. (2007). Arctic sea ice decline: Faster than forecast. *Geophysical Research Letters*, *34*(9), 9501.

Stull, R. (2008). *An introduction to boundary layer meteorology* (13th ed.). Springer.

Thorpe, S. (2007). *An Introduction to Ocean Turbulence*. Cambridge, UK: Cambridge University Press.

Wadhams, P. (2000). *Ice in the ocean*. Amsterdam, The Netherlands: Gordon and Breach Science Publishers.

Weast, R. (1971). *Handbook of Chemistry and Physics* (52nd ed.). Cleveland, Ohio: The Chemical Rubber Co.

Weeks, W. (2010). *On sea ice*. Fairbanks: University of Alaska Press.

Wettlaufer, J., Worster, M., and Huppert, H. (1997). Natural convection during solidification of an alloy from above with application to the evolution of sea ice. *Journal of Fluid Mechanics*, *344*, 291–316.

Wettlaufer, J., Worster, M., and Huppert, H. (2000). Solidification of leads: Theory, experiment, and field observations. *Journal of Geophysical Research*, *105*(C1), 1123–1134.

Widell, K., Fer, I., and Haugan, P. (2006). Salt release from warming sea ice. *Geophysical research letters*, *33*(12), L12501.